Master's Thesis

Optimal Design of Self-seeded Reflective Semiconductor Optical Amplifier for Low-cost Wavelength Division Multiplexed Passive Optical Network Applications

低コスト波長多重パッシブ光ネットワーク応用に向けたセルフシーデッド反射型半導体光増幅器の最適化設計

Zhan Wenhui (37-146889)

Supervisor: Professor Yoshiaki Nakano

Department of Electrical Engineering and Information Systems
School of Engineering, The University of Tokyo

February 2016

Chapter 1

Introduction

1.1 Access network

The development of photonics and electronics have enabled core network to have transmission as high as capacity10Tb/s per single fiber. On the other hand, the development of digital electronics and personal computers has brought various multimedia applications to uses' desktops. To ensure the quality and user experience, in the near future, at lease 30Mb/s of guaranteed bandwidth will be required at each end user [1]. Access network is the bridge between user side and core network. The ever-increasing bandwidth demand has fueled the access technologies gradually evolve from copper-based, such as digital subscriber loop, coaxial cable, to fiber-based optical access network over the years. The typical bandwidth and reach of various access technologies are listed in Tab.1 On the other hand, deployment of new fiber network needs considerable investments. The proposal of passive optical network (PON) [2] and multiplexing technologies promoted the development of optical network.

Tab.1.1

Bandwidth per user and max reach of various access technologies [3]

Service	Bandwidth/user	Max reach
ADSL	2 Mb/s (typical)	5.5 km
VDSL	20 Mb/s (typical)	1 km
Coax	2 Mb/s	0.5 km
Wi-Fi	54 Mb/s (max)	0.1 km
WiMax	28 Mb/s (max)	15 km
BPON	20 Mb/s	20 km
EPON	60 Mb/s	20 km
GPON	40 Mb/s	20 km

The topology of passive optical network (PON) is shown in Fig. 1.1 [2], PON consists of an optical line terminal (OLT) in the central office (CO), which locates at service provider side; an array of optical network units (ONU), which locate near end users. The essence of PON concept is that between OLT and ONU, only passive components are allowed in the distribution network part thus no electrical power consuming outside. As Fig.1.1 shows, a single fiber is fed from the OLT and fan out via passive splitters to distribute data to multiple ONUs. By using the passive tree topology in transmission and distribution network, PON offers significant benefits for lowering the cost and easing the maintenances of optical network system.

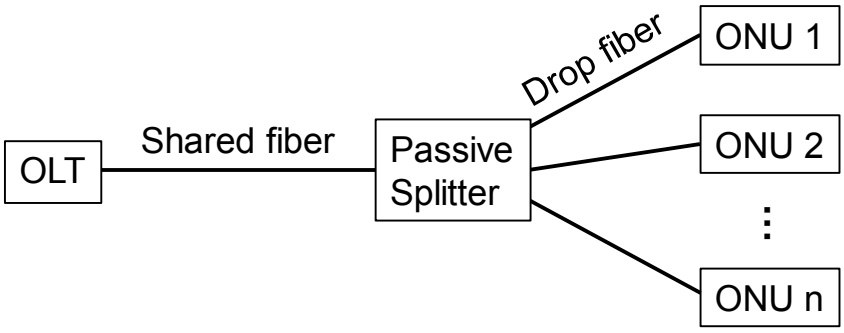

Fig. 1.1 Topology of passive optical network. (OLT: Optical line terminal, ONU: optical network unit)

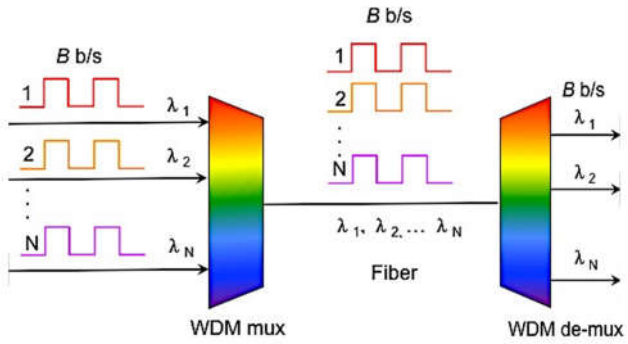

Fig 1.2 Wavelength multiplexing and demultiplexing. (WDM: Wavelength division multiplexing)

To make the best use of existing fiber, multiplexing technologies are applied on the PON system to multiplex multi-channels' data over a single fiber. There are fundamentally two ways to increase transmission capacity on a single fiber, time-division multiplexing (TDM) and wavelength-division multiplexing (WDM). Currently, most standardized PON are employing time-division multiplexing (TDM) technologies, which has been widely accepted as the current generation access network.

As the name implies, in TDM, specific time slots are assigned to individual ONUs according to their bandwidth demands. Bandwidth and devices are shared by all end users, thus in the meantime costs for each user are also lowered. The high penetration of TDM in access network is mainly due to this cost-efficiency and ability to satisfy the data rates in the short term [4]. However, with the emergence of new web-based applications, it's clear that the bandwidth should be pushed to higher date rates, and the traditional PON will out of satisfaction sooner or later, especially the ability to scale. WDM techniques are anticipated to have high performance in spite of its high cost, therefore it is preferred to be used in next-generation access [3,5].

1.2 Wavelength-Division-Multiplexed Passive Optical Network

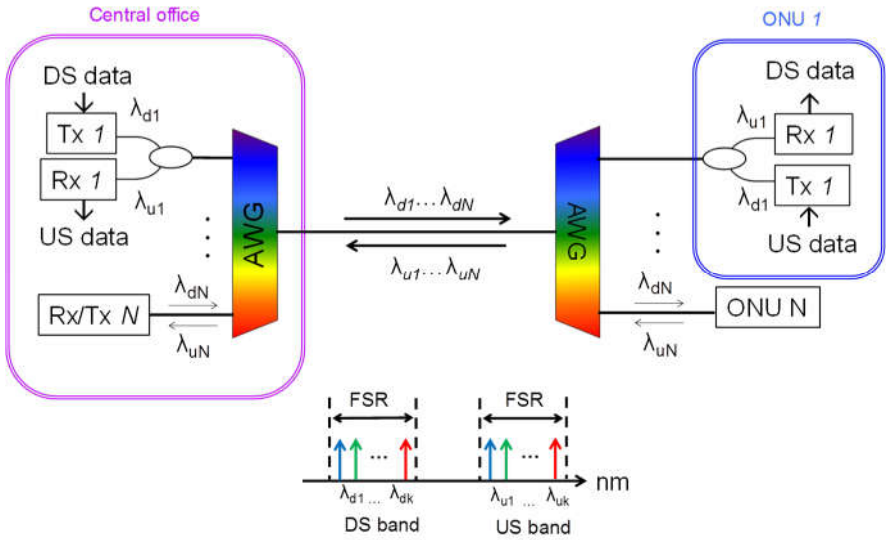

Fig. 1.3 WDM-PON architecture.
(DS: downstream, US: upstream, Tx: transmitter, Rx: receiver, AWG: Arrayed waveguide grating, ONU: Optical network unit)

The idea of WDM is transmit data at multiple carrier wavelengths (or color) simultaneously over a single fiber instead of building a dedicated fiber for each data stream (Fig.). Multiplexer combines data stream from different sources together and guild them in to a single fiber. on the other side of the fiber, the de-multiplexer routes each specific wavelength to each unique output port. The mux and de-mux are usually made of passive wavelength router, in which each port has a specific wavelength that is allowed to pass through. Arrayed waveguide grating (AWG) has been a successful

wavelength router in promoting the development of WDM-PON due to its low insertion loss, uniform wavelength spacing and temperature stability. Commercially available athermal AWG has good performance over harsh temperature from -40 to +85 °C [6].

On the basis of PON concept and WDM technologies, Fig. 1.3 shows a typical WDM-PON architecture. It comprises a central office (CO), two cyclic arrayed waveguide grating (AWG) act as mux and de-mux, a shared trunk fiber, a series of feeder fiber and multiple ONUs at subscriber premises. The data transmitted from CO to ONU is called downstream (DS), and the opposite direction is for upstream transmission. This bi-directional transmission is enabled by the two AWG deployment. The cyclic wavelength property allows the AWG to be used as both mux and de-mux in WDM-PON when the US band and DS band occupy different free spectral range (FSR) of AWG [7]. The first AWG (at CO) multiplexes the DS data and de-multiplexes US data. Similarly, the second AWG (at remote node) multiplexes the US data and de-multiplexed the DS data.

From CO to ONU, multiple transmitters generate DS data which is carried by different carrier wavelength simultaneously. The wavelengths are combined together by the AWG at CO and entered into the shared trunk fiber. The trunk fiber carries multiplexed wavelength to the other AWG. This second AWG separate the data streams according to their wavelength and guide them into destination ONUs. As a result, data stream generated by transmitters at CO is directed into their respective receivers at ONU. The upstream transmission follows the same process.

The feature of WDM-PON is that dedicated wavelength is allocated to each ONU, which on one hand, enables higher bandwidth allocation to end users, high security and easy scalability, but on the other hand, increases the cost since dedicated hardware are need for each end users.

WDM-PON systems are currently deployed in long-haul and undersea networks, local access networks still widely employ TDM-PON mainly due to WDM-PON technology has not reach its maturity for local access and the devices are unfavorable in price compared to TDM-PON. But the increasing bandwidth demand greatly drives the research on lower the cost of WDM-PON.

Among all the technologies enabling WDM-PON, the most challenging and foremost part is to achieve low-cost and low power-consuming transmitters at ONU side as users are more sensitive to cost.

In order to achieve cost-efficiency in ONU transmitters, researchers are concentrating on following aspects:

(1) Colorless. This word comes from the intuitive understanding of light that different wavelength present different colors. Colorless property means the emitted wavelength of transmitter is not fixed but tunable, thus, identical transmitters can support all wavelength channels in WDM-PON. In this viewpoint, the emitted light from transmitter is colorless. This property eases operation and maintenance and reduces cost of transmitters through volume production of one component. It is the most fundamental requirement since it is cost prohibitive to make wavelength-fixed transmitters for each ONU.

(2) Self-tuning. Only if the transmitter emits wavelength which matches with the pass band of AWG port connected to it, the transmission can be sustained. If we use tunable lasers as transmitters, the emitted wavelengths are sensitive to temperature and other ambient circumstances, conventionally, stringent wavelength tracking are needed between AWG and transmitters. The self-tuning property provides robust passive and automatic wavelength assignment.

(3) Uncooled operation. Transmitters are likely to be deployed in some harsh environment which could have temperature varies from -20 °C to 70 °C or even higher. Performance insensitive to temperature transmitters is preferable for this application.

(4) Direct modulation. This property eliminates external modulators.

Following these guidelines, many efforts have been put on low-cost transmitters, next, I will introduce several kinds of transmitters which have potential to realized one or more above-mentioned properties and facilitate WDM-PON.

1.3 Transmitters of WDM-PON

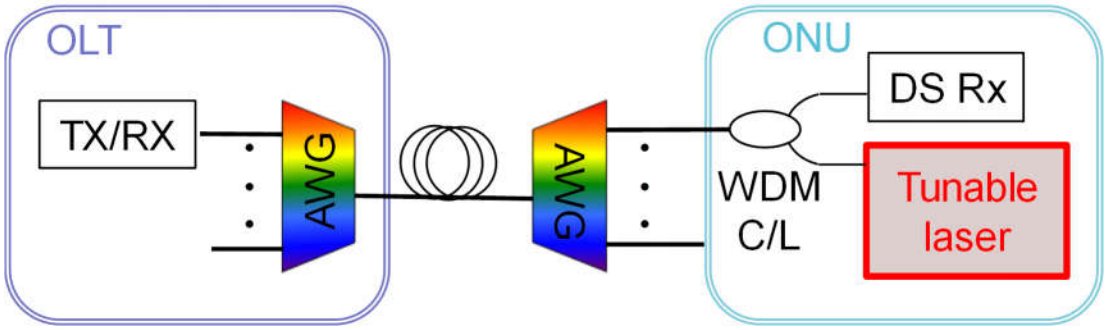

Fig. 1.4 Wavelength tunable laser as transmitters at ONU

According to the tunablity of wavelength, the optical sources have been classified into three groups. (i) wavelength-fixed lasers, (ii) wavelength tunable lasers, (iii) wavelength-selection-free light sources. The first choice can achieve long distance and high-speed transmission but it is too costly for WDM-PON due to different wavelength lasers should be deployed and separate operations as well as maintenance are need in each ONU. Vertical-cavity surface-emitting laser (VCSEL) diodes have potential for mass production due to its one-step epitaxy process [8], but 1550nm VCSEL is still in its early stage. Therefore, in the following sections, I will mainly introduce the latter two alternatives.

1.3.1 Tunable lasers

Tunable laser is a straightforward way to achieve colorless property. Identical tunable lasers can be deployed in all ONUs due to their emitting wavelength can be tuned either by tuning the temperature or varies the injected current into the LD cavity (cavity index change with temperature or with carrier injection). With strict temperature controllability, thermally tunable external cavity laser can have tunable range of several tens of nanometers [9]. Distributed Bragg reflector laser diodes (DBR-LDs) such as sampled grating and superstructure grating DBR-LDs, whose wavelength is tuned by carrier injection have achieved tuning range of 100 nm [10,11].

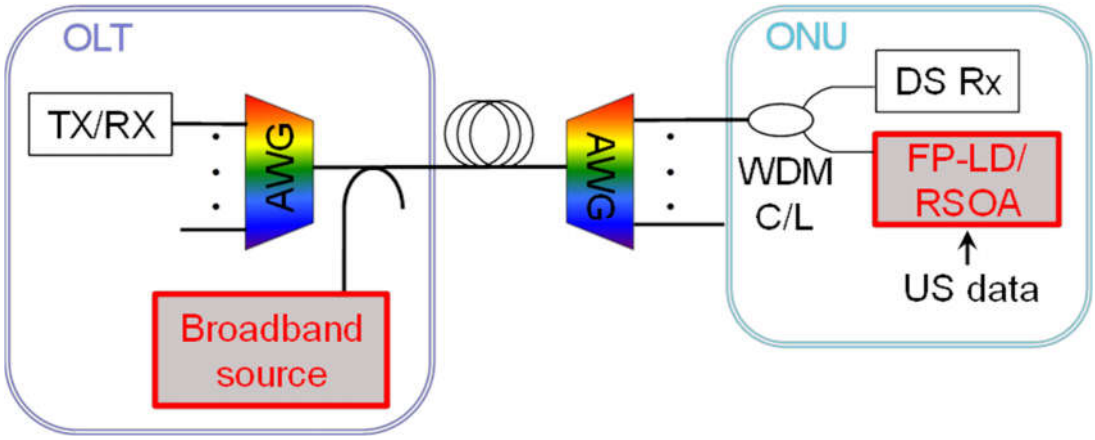

Fig. 1.5 Wavelength seeded/ injection locked scheme of RSOA/ FP-LD

Tunable lasers have best performances compared to other solutions due to its narrow linewidth and large side mode as well as noise suppression property. But we need pre-knowledge about the assigned wavelength and tune to this pre-assigned wavelength. Also, some tunable lasers need external modulators and wavelength control circuits to ensure its quality and minimize the crosstalk between different channels. It needs more cost and complex maintenances compared to other solutions.

1.3.2 Wavelength-selection-free light sources

In this scheme, optical light sources and operation conditions are identical in different ONUs as the emitted wavelength is not determined by the optical sources, but determined by the system structure.

1.3.2.1 Wavelength seeded/ Injection locking schemes

As shown the Fig. 1.5, a Fabry-Parot laser diode or a reflective semiconductor optical amplifier (RSOA) is used as transmitters at ONU. FP-LD is a multimode optical source that generates light with many wavelength components, and RSOA is an amplifier that has large gain over a wide range of wavelengths and a reflector as it has a high reflection coating at one facet. The injection locking for FP-LD and wavelength seeded scheme for RSOA need the existence of broadband light source at OLT. The centralized broadband light will be spectrally-sliced by AWG at RN and becomes a

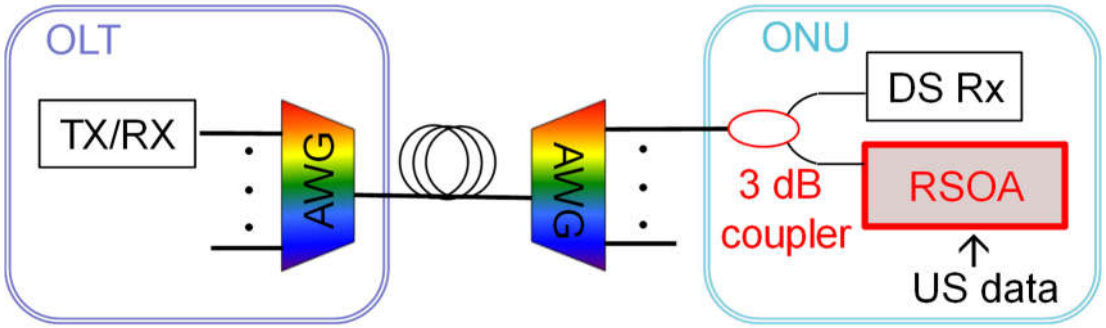

Fig. 1.6 Wavelength reuse scheme using RSOA and optical coupler.

narrow band centralized seeding light heading for the destination ONUs. When this external centralized light is injected into ONU, the FP-LD is forced to oscillate at the frequency of the external light and generate a single mode output [12]. If the transmitter is RSOA, the external seeding light is amplified and the output light has the same wavelength as incoming light [13].

Hence, the transmitting wavelength is determined externally by the incoming light. Identical FP-LDs or RSOAs can be used in all ONUs. Nevertheless, this scheme need an additional broadband light sources, which means additional power consuming. Further, the transmission performance is largely limited by amplified spontaneous emission (ASE) noise from the external light source. Also, for FP-LD transmitters, single mode lasing may need extra efforts and carefully control, because spectral sliced seeding light should match one of the lasing wavelength of FP-LD, or the gain will be low.

These schemes cannot achieve bit rate modulation as high as lasers as the modulation bandwidth is limited by the carrier lifetime in FP-LD or RSOA. Usually, <1.25 Gb/s for FP-LD and <3 Gb/s for RSOAs.

1.3.2.2 Wavelength reuse schemes

The broadband light source enables the mode-locking or wavelength seeding scheme, but the drawbacks of introducing external light source are obvious. To eliminate that, a possible method is reusing the downstream light for upstream transmission.

Fig. 1.6 shows the wavelength reuse scheme utilizing a 3-dB coupler and an RSOA at ONU [14]. The optical signal from OLT is equally split into two parts. One enters into DS receiver and the rest part enters into US transmitter to seed the RSOA. The RSOA remodulates the DS wavelength with US data, and then send US to the CO. The RSOA should be operated at deep saturation condition to suppress the amplitude modulation in the US data [15].

This scheme eliminates the need for seeding sources and use RSOA as direct modulator, making it less costly than tunable lasers and wavelength seeding/ mode-locking schemes. However, the emitted US wavelength from RSOA (transmitter) has identical wavelength as that of the DS wavelength, the performance is likely to degrade severely by the interference between DS and US carrier wavelength. To overcome this, we need to use special modulation techniques, such as phase modulation, frequency shift keying modulation [16].

1.3.3 Summary of potential transmitters

In previous sections, we have introduced several transmitters for WDM-PON applications. Tunable laser has undoubtedly the best performance of longest transmission distance and highest data rate, but it is the costliest solution among all colorless transmitters. In addition, it needs careful adjustment and stabilizers to ensure its high-quality performance. In wavelength-seeded schemes or injection-locking schemes, although the cost is lower than tunable lasers, these solutions are considered to have a short system reach and a limited upstream bitrate mainly due to the ASE noise from a broadband light source. Wavelength reuse scheme saves more energy than other solutions, but unconventional modulation formats and unconventional transceivers are needed.

Achieving colorless, self-tuning, uncooled, direct modulation in a single device is challenging for low-cost WDM-PON. Recently, a self-seeded scheme using RSOA and a partial mirror is proposed. It can be classified in the group of wavelength reuse scheme but it reuses its own US wavelength repeated by building a cavity. Looking into its structure and mechanisms, we can find it is inspired from the basic structure of laser and wavelength-seeded schemes as well as gain saturation effect used in wavelength reuse scheme. The interesting and exciting things are that it has potential to achieve colorless, robust self-tuning and uncooled operation in the WDM-PON system according to the published work and our investigation.

Therefore, we chose the self-seeded RSOA as the research topic. In the next section, the architecture and mechanism will be demonstrated in detail.

1.4 Self-seeded schemes for reflective semiconductor optical amplifiers

1.4.1 Structure of self-seeding scheme

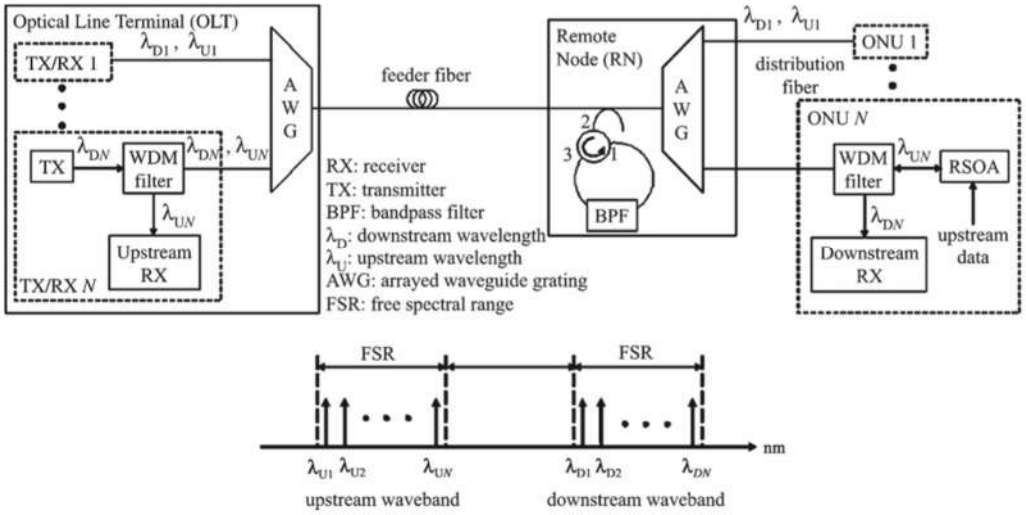

Fig 1.7 First proposal of self-seeding RSOA as directly modulated upstream transmitters in WDN-PON. [17]

In the self-seeding architecture shown in Fig 1.7 [17], each ONU has an RSOA as directly-modulated colorless upstream transmitters, and a WDM filter to combine and separate upstream and downstream wavelengths of each channel. Since the upstream and downstream signals occupy two different wavebands, two identical cyclic arrayed waveguide grating (AWG) are implemented at remote node (RN) and optical line terminal (OLT). At the RN, aside from an AWG, a passive reflective path comprised by a circulator and a bandpass filter (BPF) acts as a "partial mirror" in this scheme. The bandpass filter is centered on the upstream waveband to ensure only one wavelength will be fed back into RSOA.

Take one channel for example, with current turn on process of RSOA, broadband amplified spontaneous emission (ASE) light emitted from RSOA is first filtered by WDM filter at ONU to generate upstream waveband, and then be further filtered by AWG at RN to allocate waveband of current channel, consequently, the filtered optical spectrum has a small which is determined by the channel of AWG. Then part of the centralized light is fed back to seed RSOA itself via the passive reflective path. This specific recirculating light is called "self-seeding light". Then, RSOA can amplify the self-seeding light and emit it again to the fiber with the small peak amplified. Next, the filtered, reflected and amplified process will repeat continuously between RSOA and the partial mirror and after several round-trip, a stable narrowband light can be generated, partially for upstream transmission and the rest continuously self-seeding the RSOA. With this structure, centralized broadband light sources are avoided compared to the wavelength seeding schemes, subsequently the Rayleigh backscattering penalty from these light sources.

The main advantage of self-seeding scheme is that the wavelength is only determined by the passive component in the distribution network, referring to WDM filter, AWG and BPF in this scheme. Therefore, on one hand, this feature provides robust and stable transmission wavelength in the system. The allocated wavelength of each channel is automatically matched with the emitting wavelength of transmitter, and the temperature change at ONU will not affect the transmitted wavelength [18], which eliminates the stringent wavelength tuning and tracking between ONU and RN compared to tunable lasers. On the other hand, identical RSOAs can be utilized in all ONUs therefore colorless feature is achieved with this simple structure. Moreover, even uncooled operation can be expected if the RSOA gain and response has less temperature dependence.

In all, this structure has something in common with laser. Two mirrors, one is the high reflection facet of RSOA and the other is the passive reflective path; gain medium provided by RSOA to compensate the loss in the cavity; wavelength selective element to determine the emitting wavelength from the cavity. However, the difference is the cavity is very long, usually longer than one kilometer, therefore in direct modulation process, the modulation in the incoming light (recirculated from RN) of RSOA still has not died out, therefore the subsequent modulation is actually performed remodulation on the modulated incoming light, which in direct modulated laser theory, should suffer from large remodulation noise therefore the modulation speed is quite limited. However, experimental results show it could be modulated at much higher speed than the photon lifetime. Several experiments have successfully demonstrated data transmission of 2.5

Gb/s at C-band [19] and 10Gb/s at O-band [20] with the self-seeding structure. Obviously, we cannot use conventional laser theory to explain the high speed transmission.

1.4.2 Mechanisms of high speed modulation

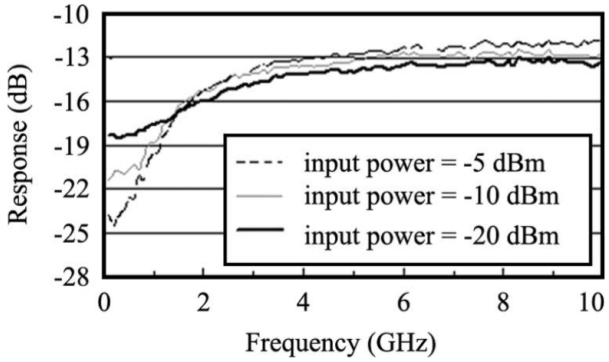

Fig 1.8 Frequency response of three different modulated input optical power of -5 dBm, -10 dBm and -20 dBm [17].

Knowing the underlying physics of such high speed modulation is important for successful operation self-seeded RSOA. Several theories have been applied to try to explain this phenomenon. All of them agree that the signal squeezing is the key to suppress modulation and then reuse the cleaned-up carriers for remodulation. Initially, the analysis of signal squeezing is mostly relied on the self-gain modulation theory of SOA [21]. Similar to a single-pass SOA, in sinusoidal frequency-swept experiment, the high-pass filter property is also observed in an RSOA [17]. As shown in Fig 1.8, the response of the input signal has strong fall-off at low frequencies, meaning the modulation in the incoming light is suppressed at this region, but at higher frequencies, there is almost a flat response therefore emitting light from RSOA still carries modulation. Moreover, with the input power increasing, the high-pass filtering effect is enhanced. Therefore, the RSOA should be operated at the low frequency region with high optical input power.

However, it is still incomplete to use SOA theory to explain RSOA features, and this explanation did not explicitly indicate the how much input power is enough and the exact conditions for the modulation canceling.

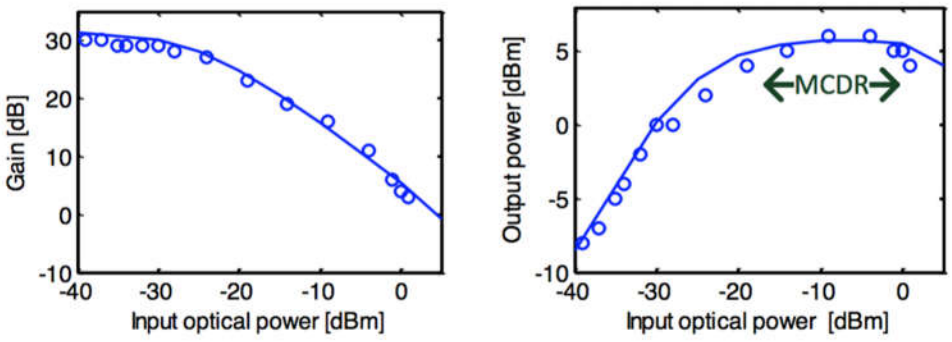

(a) (b)

Fig 1.9 Static transfer characteristics of an RSOA. (a) Optical gain as a function of input optical power, (b) Output power as a function of input power.

S. Ó Dúill, L. Marazzi, P. Parolari, et al. may have given a more convincing viewpoint to demonstrate the modulation suppression in the year of 2012 [15]. They pointed out that in an RSOA, the signal squeezing effect can not be explained from SOA theory alone, since in fact, the observed signal squeezing is much stronger than that in an SOA, which is unique in an RSOA. They also indicated that the main difference between RSOA and SOA is that, RSOA has a high reflection facet, therefore inside the RSOA, there is always has co-existence of forward and backward travelling waves. As a consequence, these two waves compete for gain from same source of carriers, making the gain saturates much stronger than a single-pass SOA whose gain saturates monotonically. As a result, it is the unique strong gain saturation effect that makes the modulation at high speed possible.

They also pointed out the operation region of modulation cancellation. Due to the strong gain saturation, in the static input-output power characteristics, a large saturation region exists, referring to the modulation cancellation dynamic regime (MCDR) in Fig 1.9 (b). Within this regime, the power variation in the input optical power cannot be transferred to the output power, which means the modulation can be suppressed. Especially, if this MCDR is flat enough, for example, smaller 1-dB power variation corresponds to output power, then we can consider that the modulation in the input power can be fully cancelled. And the output light will be almost a continuous wave (CW), which could be reused for remodulation.

1.4.3 Remodulation process of self-seeded RSOA

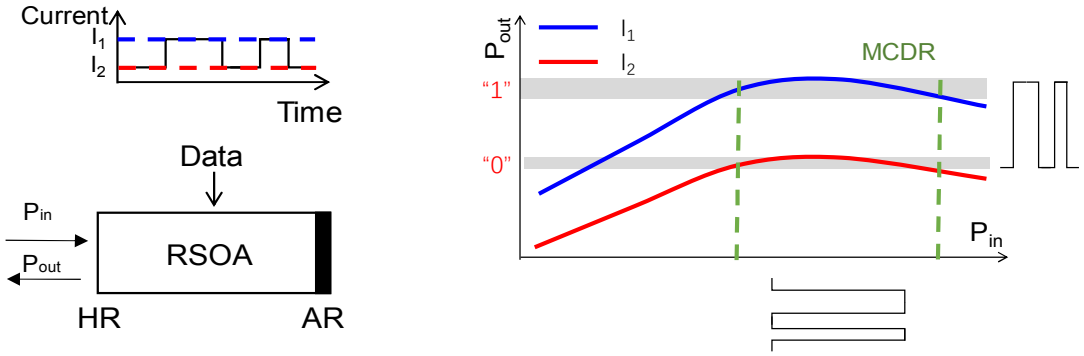

(a) (b)

Fig 1.10 Remodulation function of RSOA.
(a) Direct current modulation of RSOA, (b) remodulation process applying modulation cancellation theory.

The modulation cancellation theory gives a convincing explanation of signal squeezing. It is worth noting that in self-seeding WDM-PON, the RSOA also performs as a direct modulator, that's to say, both the modulation cancellation and the remodulation process are realized inside a single RSOA. In this thesis, we apply the modulation cancellation theory to both this two process.

The RSOA perform direct modulation through current modulation. In modulation process, we apply two level of current as lower level and higher level of binary signal to control the output amplitude of RSOA. Due to the gain saturation effect introduced in the previous section, the large MCDR exists at each level of current, meaning in each level of current, the modulation in the input power can be fully cancelled, therefore the output power of RSOA is actually only depend on the level of current, refer to the data sequence in this case.

As a brief summary, in the self-seeding scheme, the RSOA mainly performs three functions. (i) Provide gain compensation to the overall cavity loss; (ii) Allow modulation cancellation; (iii) Perform direct remodulation of the recirculating light.

Self-seeded RSOA integrates colorless, self-tuning and direct modulation together in this single device. It is a potential low-cost colorless transmitter for WDM-PON applications. The key for successful operation is the modulation canceling effect inside RSOA.

1.5 Purpose of This Research

The self-seeded configuration has widely studied during these years, and the underlying physics has been demonstrated [15]. However, the relationship between the network performance and the RSOA itself has not been fully studied yet, consequently, the full potential of self-seeded RSOA is poorly understood to the best of our knowledge.

In this study, we are aiming at explore the potential of RSOA device itself for stronger modulation canceling effect, and use the self-seeded RSOA for higher temperature, higher bit rate transmission. To accomplish that, we built a numerical model to reproduce the gain saturation effect inside RSOA, subsequently, we rely on both numerical and experimental results to investigate the influence of RSOA design on the performance of self-seeding system. Then, we give our prediction of the optimal RSOA design for self-seeded WDM-PON transmitters and verified the prediction by 2.5 Gb/s self-seeded transmission experiment. Finally, we apply this optimal length to uncooled (70 °C) and higher bit rate (10 Gb/s) system.

1.6 Outline of This Thesis

In this thesis, we present a detailed numerical and experimental demonstration of self-seeded RSOA for low-cost WDM-PON transmitters.

The contents in each chapter are organized as follows:

In chapter 1, we briefly introduce the WDM-PON composition and the current challenges for wide adoption of WDM-PON. We introduce several kinds of transmitters and compared them with each other. In the final part, we introduce the self-seeded RSOA as transmitters and demonstrated its working principles in detail.

In chapter 2, we build a numerical model of RSOA. Since gain competition is the most important factor to affect the gain dynamics of RSOA, our numerical model contains this factor into the model and reproduces the modulation canceling effect shown by RSOA.

In chapter 3, we use the model to investigate factors which have influence on modulation canceling effect from the aspect of operation conditions and RSOA design. We investigate in influence of optical input power, injected current, temperature and RSOA length. Further, we carry out a comprehensive analysis on these influence factors

and finally derive our prediction of the optimal RSOA design for large range of operation conditions.

In chapter 4, we show the experimental results which verify our numerical prediction. Also, we apply this derived optimal RSOA design for higher temperature conditions and higher bit rate transmission systems.

In chapter 5, we summarize our work and make conclusions of this study.

Chapter 2

Numerical Model of RSOA

In this chapter, I will introduce the numerical model in detail. We first show the rate equations for an RSOA device, and then give our explanation on how to solve these rate equations.

2.1 Modified rate equation for RSOA

The RSOA model is based on the well-known carrier rate equations and wave propagation equations of a bidirectional SOA [22]. We modified them to contain the mutual effect between counter-propagating waves within RSOA.

2.1.1 Carrier rate equation

Carrier rate equation is used to describe how an injected current results in an optical output. Due to charge neutrality, i.e., the electron density equals the hole density, we only track the electron density, N in our study.

We neglect the carrier diffusion due to the almost uniform distribution of carrier density at the cross-section of active layer. According to the mechanisms of generating and draining the carrier in active region, the electron equation can be written as:

$$\frac{dN}{dt} = \frac{I}{qV} - R(N) - R_{st} \tag{2-1}$$

The first term in the right side is the carrier generation rate due to current injection, where I/q is the electrons injected into the active region per second, V is the volume of the active region. The other two terms in the right side is related with various recombination processes. The second term refers to the natural or non-stimulated carrier decay processes, which can be expressed in a power series of carrier density, N, in the form of

$$R(N) = AN + BN^2 + CN^3 \tag{2-2}$$

Where A is the nonradiative recombination coefficient, B is called the bimolecular recombination coefficient and C is the Auger recombination coefficient.

The third term in equation (2-1) is the net stimulated recombination rate, which represents the gain process of photons due to stimulated electron-hole recombination. Therefore, we use the incremental gain per unit length Δz, g, to describe the growth of photon density, N_p, through the gain medium:

$$N_p(z+\Delta z) = N_p(z)e^{g\Delta z} \tag{2-3}$$

Using the proximity relation of exponential function, $e^{g\Delta z} \approx 1+g\Delta z$, the stimulated recombination term can be rewritten as,

$$(\frac{dN_p}{dt})_{gen} = R_{st} = v_g g N_p \tag{2-4}$$

Where v_g is the group velocity.

Thus, now the carrier rate equation can be write in the following equation [23]:

$$\frac{dN}{dt} = \frac{I}{qV} - (AN + BN^2 + CN^3) - V_g g N_p \tag{2-5}$$

2.1.2 Travelling wave equation

The propagation of electromagnetic field inside the RSOA is governed by the travelling wave equation, which is derived from the Maxwell equation.

For counter propagating signal field, the wave equation is found to be [24]

$$\pm\frac{\partial E^{\pm}(z,t)}{\partial z} + \frac{1}{v_g}\frac{\partial E^{\pm}(z,t)}{\partial t} = \frac{1}{2}(\Gamma g - \alpha_{\text{int}})E^{\pm}(z,t) + j\Gamma k_0 \Delta n E^{\pm}(z,t) \tag{2-6}$$

Where the $E(z,t)$ is the electrical field of the optical signal, Γ is the confinement factor, α_{int} is the internal loss, k_0 is the wave number, Δn is the refractive index change due to current injection, + represents the forward propagating wave and – corresponds to backward propagating wave. We can separate the optical power component and phase component by writing the $E(z,t)$ into

$$E(z,t) = \sqrt{P(z,t)}e^{-j\phi(z,t)} \tag{2-7}$$

Substitute Eq. (2-7) into Eq. (2-6), the wave equation becomes

$$\pm\frac{\partial P^{\pm}(z,t)}{\partial z} + \frac{1}{v_g}\frac{\partial P^{\pm}(z,t)}{\partial t} = (\Gamma g^{\pm} - \alpha_{\text{int}})P^{\pm}(z,t) \tag{2-8}$$

$$\pm\frac{\partial\phi(z,t)}{\partial z}+\frac{1}{v_g}\frac{\partial\phi(z,t)}{\partial t}=-\frac{\Gamma k_0\Delta n}{\phi} \tag{2-9}$$

Moreover, the optical power can be linked to photon density through the relationship of,

$$P=N_{ph}\hbar\omega\cdot wdv_g \tag{2-10}$$

Where $\hbar\omega$ is the energy of a single photon, w is the width of active region and d is the thickness of active region.

For the ASE field, we describe the spontaneous emission in terms of power, thus the wave equation is [25]

$$\pm\frac{\partial\rho_{ASE}^{\pm}(z,t)}{\partial z}=(\Gamma g-\alpha_{\text{int}})\rho_{ASE}^{\pm}(z,t)+\rho_{spon}(z,t) \tag{2-11}$$

Where $\rho_{ASE}^{\pm}$ is the amplified spontaneous emission power spectral density of forward and backward propagating ASE waves, ρ_{spon} is the spontaneous emission power spectral density. Eq. (2-10) describes the generated spontaneous emission is amplified as it propagates inside the RSOA.

2.1.3 Gain equation

In laser theory, the material gain is suggested to be expressed as a linear function of carrier density [23]

$$g(N(z,t))=a_0(N(z,t)-N_0) \tag{2-12}$$

Where a_0 is the differential gain coefficient and N_0 is the carrier density at transparency. However, in RSOA, the photon density also affects more on material gain. Experimental results show that for higher photon density, the gain decreases and the gain in RSOA starts to saturate from a low optical input power compare to that in a SOA. In the previous section, we have introduced that the strong gain saturation effect in RSOA is due to the co-existence of forward and backward propagating waves, to contain the mutual effect of two waves, we modify the gain into

$$g^{+}(z,t)=\frac{a_0(N-N_0)}{1+\varepsilon_{11}n_{ph}^{+}+\varepsilon_{12}n_{ph}^{-}} \tag{2-13}$$

$$g^{-}(z,t)=\frac{a_0(N-N_0)}{1+\varepsilon_{22}n_{ph}^{-}+\varepsilon_{21}n_{ph}^{+}} \tag{2-14}$$

Where g^{+} and g^{-} are the material gain for forward traveling wave and backward traveling wave, respectively. ε_{11} and ε_{22} are the self-gain saturation coefficient and ε_{12}

and ε_{21} are the cross-gain saturation coefficient. The cross-gain saturation coefficient are always assumed to be 2 times of self-gain saturation coefficient [26].

2.1.4 Summary of rate equations

In sum, we use following set of equations to describe the carrier dynamics and amplification as well as gain dynamics inside RSOA.

For carrier: $$\frac{dN}{dt} = \frac{I}{qV} - (AN + BN^2 + CN^3) - V_g g N_{ph} \tag{2-15}$$

For signal: $$\pm\frac{\partial P^{\pm}(z,t)}{\partial z} + \frac{1}{v_g}\frac{\partial P^{\pm}(z,t)}{\partial t} = (\Gamma g^{\pm} - \alpha_{\text{int}})P^{\pm}(z,t) \tag{2-16}$$

For noise: $$\pm\frac{\partial \rho_{ASE}^{\pm}(z,t)}{\partial z} = (\Gamma g - \alpha_{\text{int}})\rho_{ASE}^{\pm}(z,t) + \rho_{spon}(z,t) \tag{2-17}$$

For forward gain: $$g^{+}(z,t) = \frac{a_0(N - N_0)}{1 + \varepsilon_{11}N_{ph}^{+} + \varepsilon_{12}N_{ph}^{-}} \tag{2-18}$$

For backward gain: $$g^{-}(z,t) = \frac{a_0(N - N_0)}{1 + \varepsilon_{22}N_{ph}^{-} + \varepsilon_{21}N_{ph}^{+}} \tag{2-19}$$

2.2 Solution of rate equations

We use finite difference method to deal with the carrier rate equations and produce a time domain RSOA model as depicted in Fig. 2.1. In the RSOA model, the total device is sliced into *m* spatial sections. If the length of each section is small enough, we can consider that the carrier density and bi-directional gain remain constant within each section. But in different sections, the carrier density is varied due to wave propagation. The propagating optical field contains signal and ASE. The ASE is the main noise source; it affects the RSOA performance especially at low stimulated emission power.

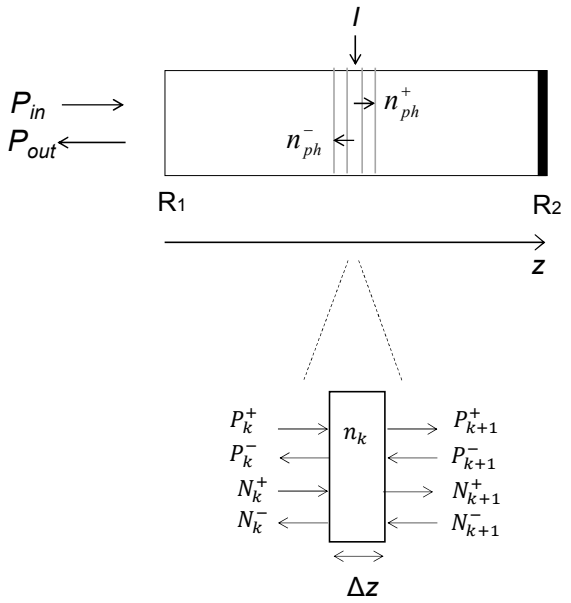

Fig. 2.1 RSOA simulation schematics.

2.2.1 Derivation of recurrence relations

We first deal with Eq. (2-15). According to finite difference method, the differential term in the left hand side can be estimated by the difference of carrier density *N* between next time slot and current time, that is

$$\frac{dN(z,t)}{dt} = \frac{N(z,t+\Delta t)-N(z,t)}{\Delta t} = \frac{N_k(t+\Delta t)-N_k(t)}{\Delta t} \tag{2-20}$$

We use subscript *k* to represent the *k*th section. Substitute Eq. (2-20) into Eq. (2-15) and leave only $N_k(t+\Delta t)$ on the left hand side, therefore, we have the recurrence relation,

$$N_k(t+\Delta t) = N_k(t) + \Delta t[\frac{I(t)}{qV} - R(N_k) - v_g g_k^+(N_{ph,k}^+ + N_{ase,k}^+) - v_g g_k^-(N_{ph,k}^- + N_{ase,k}^-)] \tag{2-21}$$

With this equation, carrier density of *k*th section in the next moment can be deduced from the current situation. The carrier density of the *(k+1)*th section is determined analogously by knowing the information of carrier density, injected current, gain and photon density at last moment.

It is hard to derive the recurrence relation of Eq. (2-15) by only using finite differential method. Therefore, we simplify it by making the transformation [27]

$$\tau = t - \frac{z}{v_g} \tag{2-22}$$

Then the solution of Eq. (2-15) is

$$P_{k+1}^{+}(t+\Delta t) = P_k^{+}(t)e^{(\Gamma g_k^{+}(t)-\alpha)\Delta z} \tag{2-23}$$

$$P_{k-1}^{-}(t+\Delta t) = P_k^{-}(t)e^{(\Gamma g_k^{-}(t)-\alpha)\Delta z} \tag{2-24}$$

These two equations give the recurrence relation of optical signal power in last segment and next segment, that's to say, the power in *(k+1)*th segment can be derived by the information in kth section. By this analogy, optical power in *(k+2)*th segment can also be known from *(k+1)*th segment, so as further segments. Therefore, these equations give us an intuitive understanding of wave propagating process in RSOA.

For the ASE noise propagation, it is valid to use the simple finite differential method as what we did to the carrier rate equation. we simply use the forward difference quotients to estimate the differential term, thus, for the forward propagating ASE,

$$\rho_{ase,k+1}^{+} = [1+(\Gamma g_k^{+} - \alpha)\Delta z]\rho_{ase,k}^{+} + \rho_{spon,k}\Delta z \tag{2-25}$$

Since Δz is sufficiently small, we can write the first term in the right hand side into an exponential term according to

$$e^{a\Delta z} \approx (1 + a\Delta z) \tag{2-26}$$

Therefore, Eq.(2-25) becomes

$$\rho_{ase,k+1}^{+} = \rho_{ase,k}^{+} e^{(\Gamma g_k^{+} - \alpha)\Delta z} + \rho_{spon,k}\Delta z \tag{2-27}$$

Consider the physical meaning of this equation, it tells us that in each segment, the ASE power has two contributions: the first contribution is shown by the first term in the right hand side, it is the amplified input noise which follows the same process as signal

propagation in Eq. (2-23,24), the second contribution is shown by the second term in the right hand side, it is the spontaneous emission component generated from that section. For a section of length Δz, the generated spontaneous emission spectral power density within that section is given by [28]:

$$\rho_{spon,k}\Delta z = \eta_{sp}(G_k - 1)h\nu \tag{2-28}$$

Where η_{sp} represents the spontaneous emission factor, G_k represents the single pass gain of that section, equal to $e^{(\Gamma g_k^+ - \alpha)\Delta z}$ here. In out model, we assume a constant noise power spectral density over an optical bandwidth B_0, thus, the recurrence relation of ASE power can be written as,

$$P_{ase,k+1}^+ = P_{ase,k}^+ e^{(\Gamma g_k^+ - \alpha)\Delta z} + \eta_{sp}(e^{(\Gamma g_k^+ - \alpha)\Delta z} - 1)h\nu B_0 \tag{2-29}$$

Similarly, for the backward propagating ASE,

$$P_{ase,k-1}^- = P_{ase,k}^- e^{(\Gamma g_k^- - \alpha)\Delta z} + \eta_{sp}(e^{(\Gamma g_k^- - \alpha)\Delta z} - 1)h\nu B_0 \tag{2-30}$$

With appropriate boundary conditions, waves can propagate repeatedly inside RSOA. In our model, the RSOA is illuminated by a CW source with optical power P_{in}, and the reflection coefficient for front and rear facet are R_1 and R_2, respectively, therefore, the boundary conditions are:

$$P_0^+ = (1 - R_1)P_{in} + R_1 P_0^- \tag{2-31}$$

$$P_m^- = R_2 P_m^+ \tag{2-32}$$

$$N_0^+ = R_1 N_0^- \tag{2-33}$$

$$N_m^- = R_2 N_m^+ \tag{2-34}$$

Where m means the device has been sliced into m sections.

The power of output signal and ASE are,

$$P_{out}(t) = (1 - R_1)P_0^- \tag{2-35}$$

$$N_{out}(t) = (1 - R_1)N_0^- \tag{2-36}$$

For the measured input power and output power, the fiber coupling loss should be considered.

2.2.2 Summary of recurrence relation

In sum, we use the following equations to calculate the carrier density, optical power and material gain section by section, hence simulate the wave propagation process inside RSOA. With appropriate boundary conditions in the two facets of RSOA and initial values listed in the last section to starting this iteration, we can obtain the resulting output from RSOA.

$$g_k^{\pm}(t) = \frac{a_0(N_k(t) - N_0)}{1 + \varepsilon_{11}(N_{ph,k}^{\pm}(t) + N_{ase,k}^{\pm}(t)) + \varepsilon_{12}(N_{ph,k}^{\mp}(t) + N_{ase,k}^{\mp}(t))} \tag{2-37}$$

$$P_{k\pm1}^{\pm}(t + \Delta t) = P_k^{\pm}(t) e^{(\Gamma g_k^{\pm}(t) - \alpha)\Delta z} \tag{2-38}$$

$$P_{ase,k\pm1}^{\pm}(t + \Delta t) = P_{ase,k}^{\pm}(t) e^{(\Gamma g_k^{\pm}(t) - \alpha)\Delta z} + \eta_{sp}(e^{(\Gamma g_k^{\pm}(t) - \alpha)\Delta z} - 1) h\nu B_0 \tag{2-39}$$

$$N_k(t + \Delta t) = N_k(t) + \Delta t[\frac{I(t)}{qV} - R(N_k) - v_g g_k^{+}(N_{ph,k}^{+} + N_{ase,k}^{+}) - v_g g_k^{-}(N_{ph,k}^{-} + N_{ase,k}^{-})] \tag{2-40}$$

$$P_0^{+} = (1 - R_1)P_{in} + R_1 P_0^{-} \tag{2-41}$$

$$P_m^{-} = R_2 P_m^{+} \tag{2-42}$$

$$P_{out}(t) = (1 - R_1)P_0^{-} \tag{2-43}$$

$$N_{out}(t) = (1 - R_1)N_0^{-} \tag{2-44}$$

Chapter 3

Numerical study of RSOA

In this chapter, I will first derive the values of parameters we used in the model. Then I will use the numerical model to reproduce the modulation canceling effect (large gain saturation effect) of RSOA. Then, we do some preliminary studies on influence factor of this gain saturation effect. With numerical study at various input optical power, multiple bias current and two different ambient temperatures for RSOAs with different lengths, we indicate that there exists a critical length to achieve strong modulation cancellation effect.

3.1 Description of RSOA chips

Before we using the numerical model for further investigation, we should first determine the value of parameters used in the model. As introduced in the last chapter, with a certain continues input power, our numerical model can derive the corresponding output power. Therefore, we can derive the parameters by fitting to the experimental results.

First, we measure the static input versus output power transfer characteristics of RSOA chip. The schematics of RSOA chip we employed are shown in Fig. 3.1 and Fig. 3.2. From the top view, there are anti-reflection (AR) coating at one facet, and high-reflection (HR) coating at the other facet. The waveguide has a 7° curve near anti-reflection facet to further avoid reflection from AR facet, thus avoid FP cavity effect of the device. From the cross section shown in Fig. 3.2, the active layer employ InGaAlAs multi-quantum well. We choose InGaAlAs as active medium due to its temperature stability. The conventional InGaAsP material usually have poor temperature characteristics, the reason is partly due to poor electron confinement due to

the small conduction band offset ($\Delta E_c = 0.4\,\Delta E_g$). Compared to that, InGaAsAl has larger conduction band offset($\Delta E_c = 0.72\,\Delta E_g$) [29], therefore a strong electron confinement. In this study, we also want to investigate the uncooled characteristics of RSOA, so InGaAlAs should be better for WDM-PON applications.

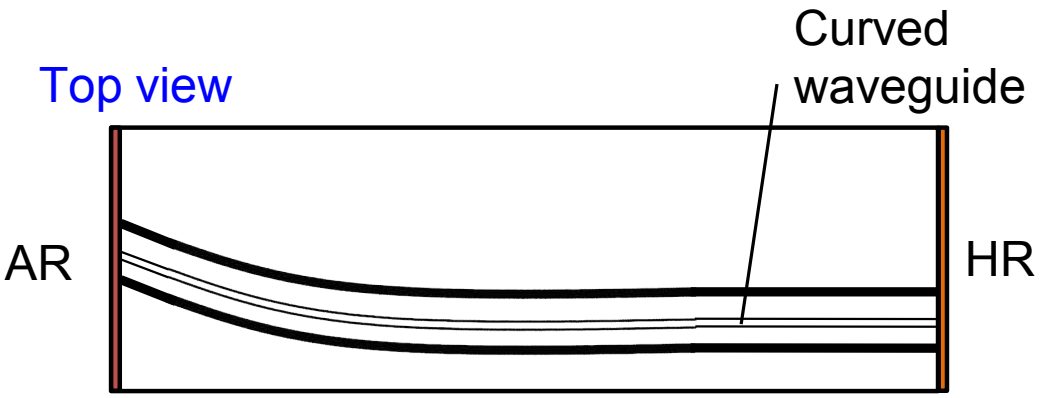

Fig. 3.1 Cross section of RSOA chip

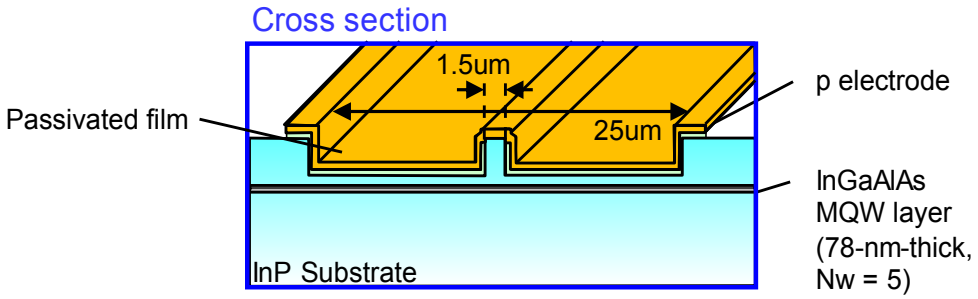

Fig. 3.2 Cross section of RSOA chip

3.2 Static characterization of RSOA

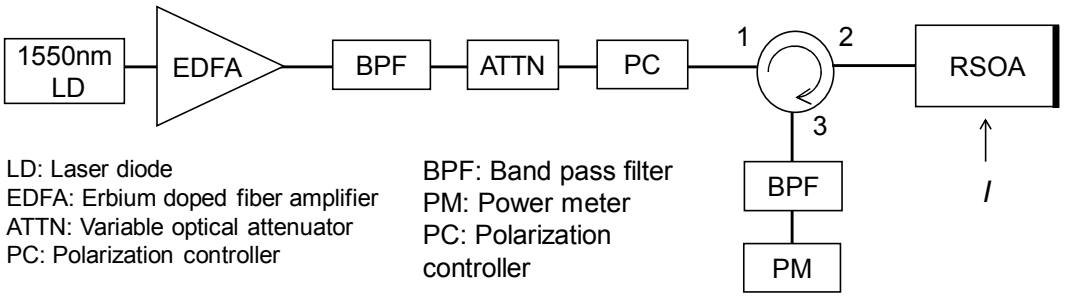

Fig. 3.3 Experimental setup of static characterization

We use the setup shown in Fig. 3.3 to experimentally characterize the input versus output power curve of RSOA.

The RSOA we used in this experiment has length of 1.0mm with the ambient temperature is 25 °C, and it is biased at direct current, the input light is emitted from a laser diode with wavelength of 1550 nm. The input power is controlled by an optical variable attenuator, and the corresponding output power is recorded by a power meter. We use the EDFA after LD since its maximum output is 10 dBm, and the EDFA can amplify this light so that we can broaden the region of input power. The RSOA has high polarization dependent gain, therefore we use the polarization controller to maximum the gain in RSOA.

We measured the input-output power curve at several different levels of bias current as shown in the dash line in Fig. 3.4 Then we carefully adjust the value of parameters used in our numerical model. As shown in solid line in Fig.3.4, we achieve reasonable agreement between experiment and simulation at different level of current. In Fig., the optical loss in the input path and output path has been considered, therefore, the value shown in the figure is fiber-to-fiber power.

Therefore, we can determine the parameters. The parameters we used in the model are shown in Tab. 3.1.

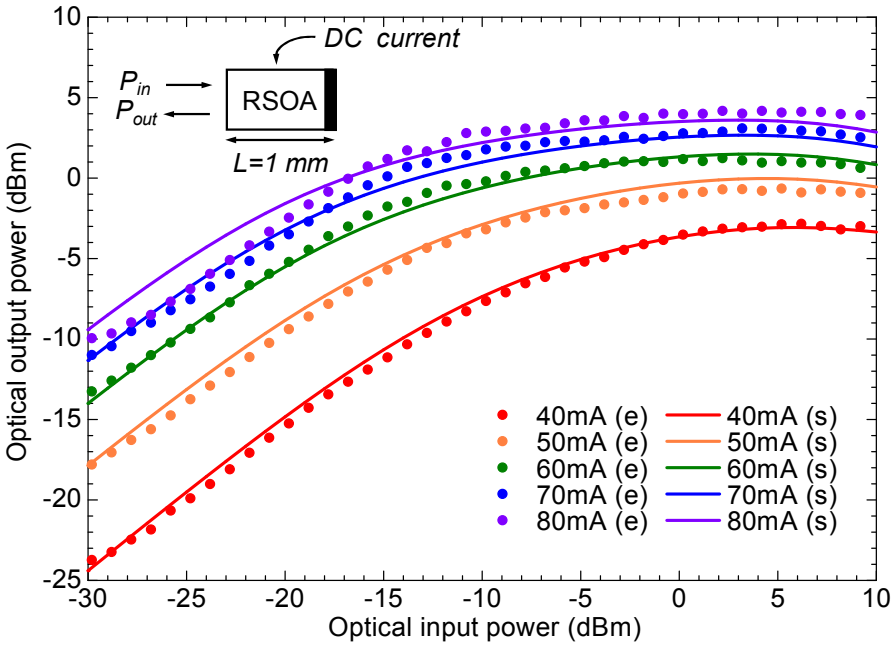

Fig. 3.4 Static input power versus output power transfer characteristics of RSOA with length of 1 mm. Dash line: experimental results. Solid line: simulation results.

Tab. 3.1 Parameters used in the model (25°C)

Parameter	**Symbol**	**Value**
Wavelength	λ	1550 nm
Active region width*	w	1.5 μm
Active layer thickness*	d	78 nm
Cavity waveguide loss*	α	21 cm^{-1}
Coupling loss from/to lensed fiber †	L_c	5 dB
Reflectivity at front facet*	R_1	0
Reflectivity at back facet*	R_2	1
Confinement factor*	Γ	11.1%
Gain constant †	a	3.2×10^{-16} cm^2
Carrier density at transparency †	n_0	6.0×10^{17} cm^{-3}
Group refractive index*	N_g	3.4
Nonradiative recombination rate †	A	5.0×10^{8} s^{-1}
Bimolecular recombination rate †	B	2.0×10^{-10} cm^3s^{-1}
Auger recombination rate †	C	1.2×10^{-28} cm^6s^{-1}
ASE bandwidth	B_0	1.5×10^{13} Hz
Self-saturation coefficient †	ε_{11}	1.12×10^{-16} cm^3
Cross-saturation coefficient †	ε_{12}	2.24×10^{-16} cm^3
Mesh size along z	Δz	5 μm

* Measured or derived by other methods † Fitted to experimental results

3.3 Preliminary study with the numerical model

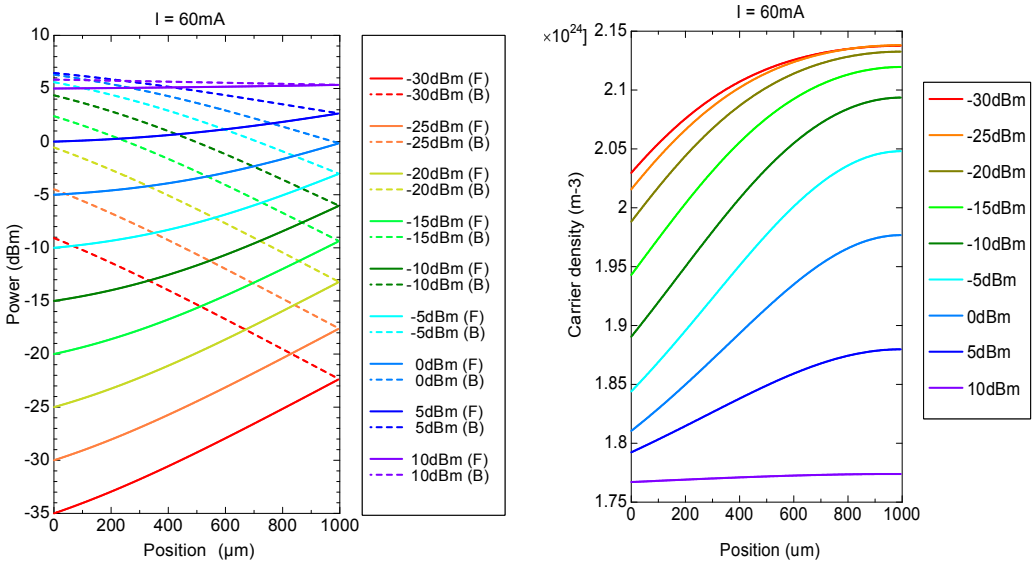

(a) Optical power distribution (b) Carrier density distribution

Fig. 3.5 Carrier density and photon density distribution inside RSOA with 1.0 mm long length at injected current of 60mA. (F: forward, B: backward)

With the derived parameters, we use the model to study influence of operation conditions on the gain dynamics inside RSOA. Since we calculate carrier density and photon density of each section in the model, we can simulate the photon and carrier distribution inside RSOA.

Fig. 3.5 shows the carrier and photon density distribution in a RSOA with 1.0-mm-long length. The injected current is fixed at 60mA in each case, and the input optical power varies from -30 dBm to 10 dBm. In the figure, we observe the amplifying and saturation phenomenon of optical power. With low optical input power, the forward and backward waves are almost amplified linearly, while with higher optical input power, the gain even changes along length and consequently, the lines in Fig. 3.5 (a) become curved. On the other hand, comparing amplification among different input power, we can see the gain decreases in the high input power. The carrier distribution shown in Fig 3.5 (b) is consistent with photon distribution that higher photon density corresponds to lower carrier density and vice versa. Moreover, the carrier density

distribution is not uniform inside the RSOA, we observe lower density in the front facet and higher in the rear facet due to the non-uniform distribution of optical power.

Optical input power affects the gain dynamics, and so as the injected current. As shown in Fig. 3.6, the optical input power is fixed at -10 dBm, and the injected current varies from 40mA to 160mA. Higher injected current results in higher amplification of light, but also easy to have the gain degradation inside RSOA.

Then we investigate the influence of length on the gain dynamics, in this case, we vary the length of RSOA but keep the current density the same for each length. The results are shown in Fig. 3.7, longer length has higher optical output power due to longer length to perform amplification in the case of same carrier density, and longer length are easier to have gain degradation inside the chip due to high optical power.

By now, we have shown the influence of optical input power, injected current and length of RSOA on the power and carrier distribution inside the device. All these mentioned three factors can affect the gain dynamics inside the RSOA, therefore, change the modulation cancellation dynamic region (MCDR), which has been introduced in Chapter 1, and consequently, affect the performance of the RSOA in a self-seeded system.

We can intuitively understand how the input power, injected current and length of RSOA affect the MCDR by referring to Fig.3.4 and Fig. 3.8. As shown in Fig.3.4, higher injected current made the right side of the curve flatter, meaning under higher injected current, the MCDR in increased. In Fig. 3.8, we show the simulation results of static input-output curves of several lengths at the same injected current. We keep the injected current same since that the MCDR is the result of gain competition between counter-propagation waves from the same sources of carrier, therefore, we inject similar numbers of carrier. In short length, the saturation is not enough so that the output power start to saturate at relatively high input power. While in long length, due to more space to amplify, the gain saturates so strongly that the input power decreases too fast. So it must exist an intermediate length, at which, the gain saturates gradually, and as a result, a large flat region can be obtained with this optimal length.

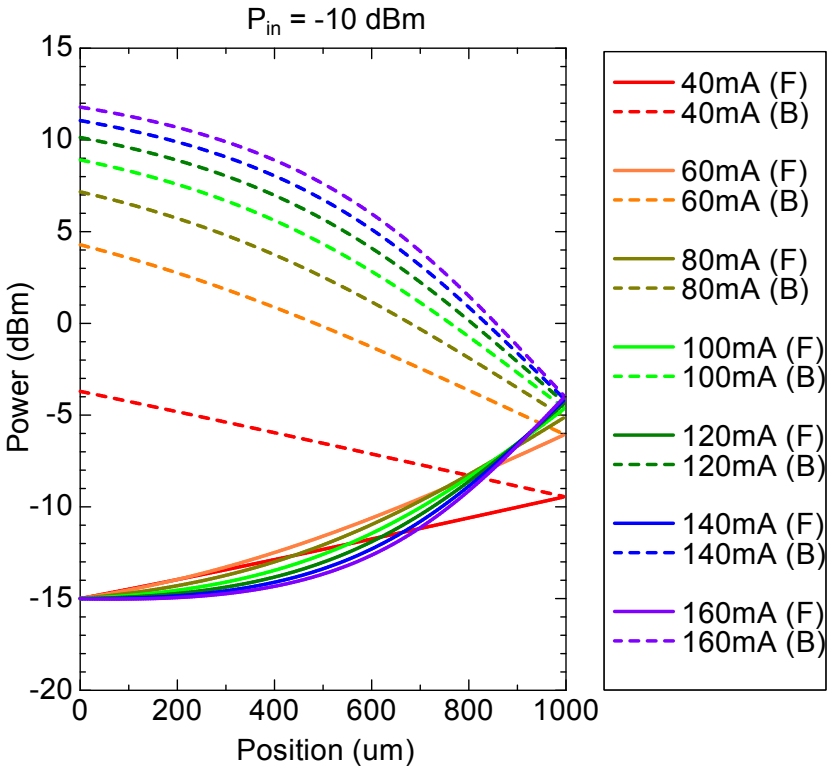

(a) Optical power distribution

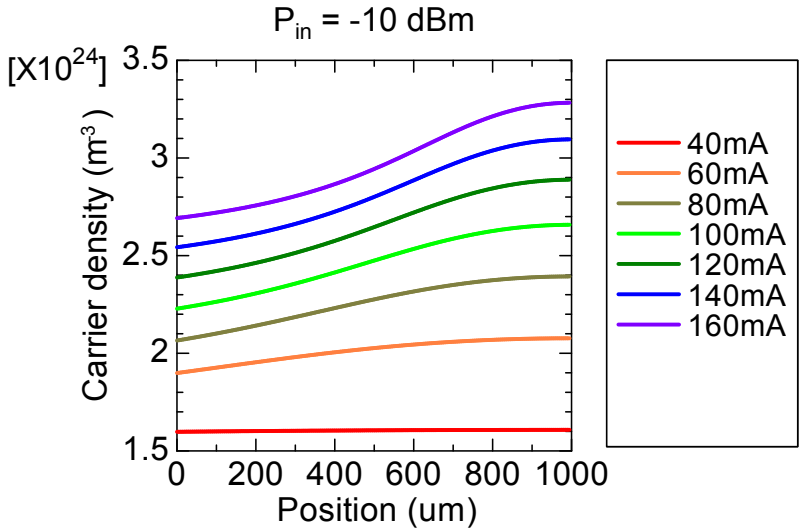

(b) Carrier density distribution

Fig. 3.6 Optical power and carrier density distribution with RSOA length of 1.0 mm at input power of -10 dBm. (F: forward, B: backward)

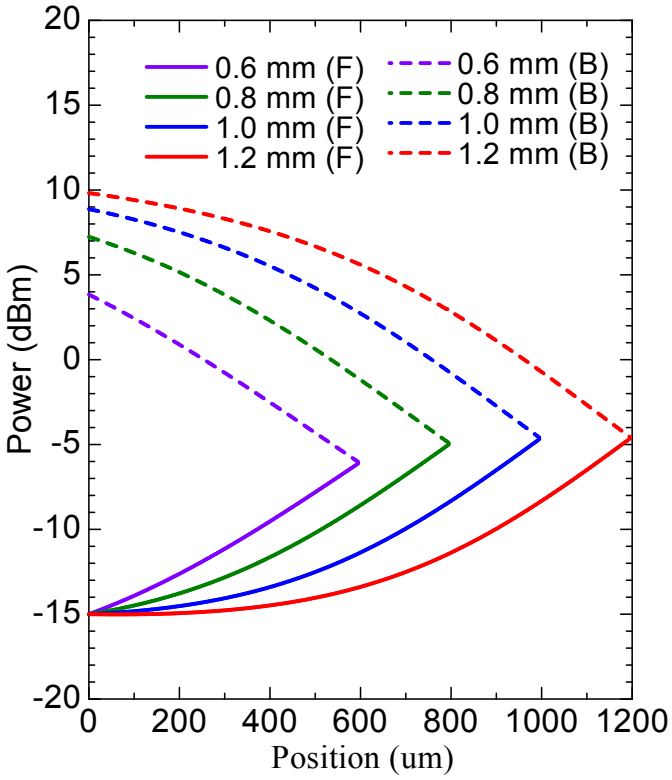

(a) Optical power distribution

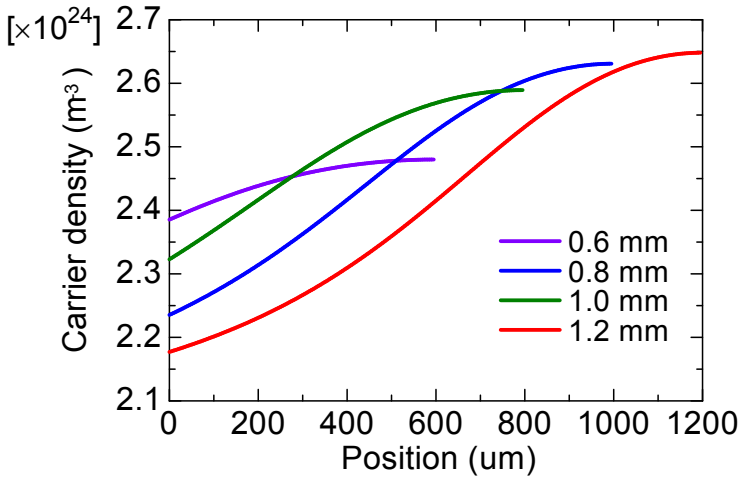

(b) Carrier density distribution

Fig. 3.7 Power and carrier density distribution with RSOA of length of 0.6 mm, 0.8 mm, 1.0 mm and 1.2 mm. The corresponding injected current is 60mA, 80mA, 100mA and 120 mA.

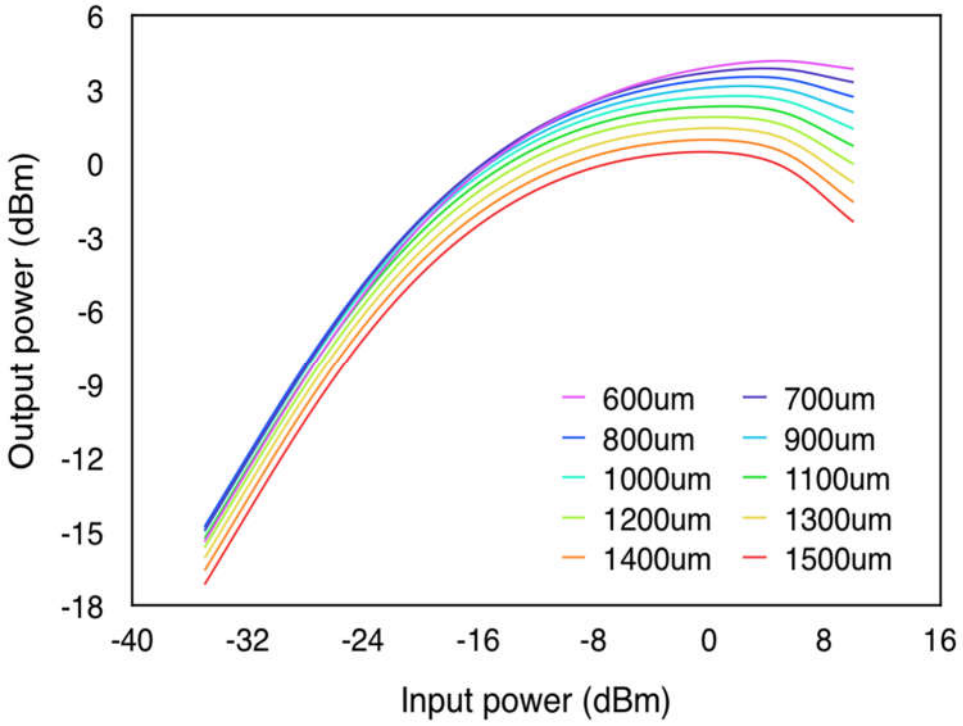

Fig. 3.8 Simulation results of input versus output curves with different RSOA length at injected current of 100mA.

However, it is easy to recognize that the analysis of modulation cancellation effect of RSOA is incomplete only with Fig.3.4 and Fig.3.8 They just give us an intuitive understanding of MCDR, we need a more comprehensive analysis on the influence of injected current, optical input power and RSOA length. We will show the demonstration in the following sections.

3.4 Static characteristics of RSOA with different length, at different ambient temperature.

In this section, other than the influence of RSOA length, input optical power and injected current, we also investigated the temperature dependence since we expect the uncooled operation of RSOA in the self-seeded system.

As we know, input optical power and injected current should not change the material parameters used in the model, but temperature could change them. Therefore,

at the same temperature, other than length, we can use the same material parameters, while at different temperatures, we need to derive new value of parameters.

The procedure to derive parameters at higher temperature follows the same steps as shown in section 3.2, but we have more variables in this measurement. At each temperature, we measure the static transfer characterization of RSOA with different length, at various input optical power and various level of injected current. We prepared three RSOA sample with length of 0.6 mm, 1.0 mm and 1.8 mm, the temperature for characterization is 25°C, 50°C.

As shown in Fig. 3.9 and Fig. 3.10, in all cases including different lengths, input power and temperature, we achieve reasonable agreements using the parameters listed in Tab.3.2. Therefore, we believe the derived parameters are accurate and can reflect the true conditions inside RSOA.

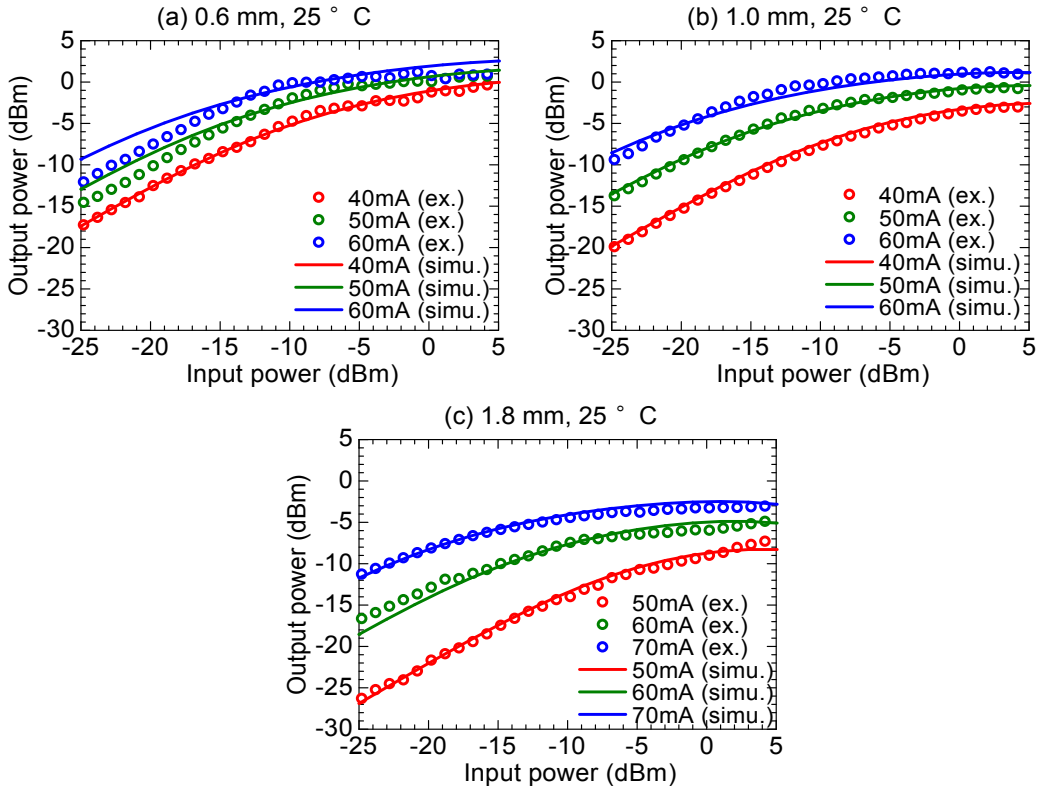

Fig. 3.9 Static input versus output characteristics of RSOA with length of 0.6 mm (a), 1.0 mm (b) and 1.8 mm (c) at the temperature of 25 °C. (ex.: experimental result,

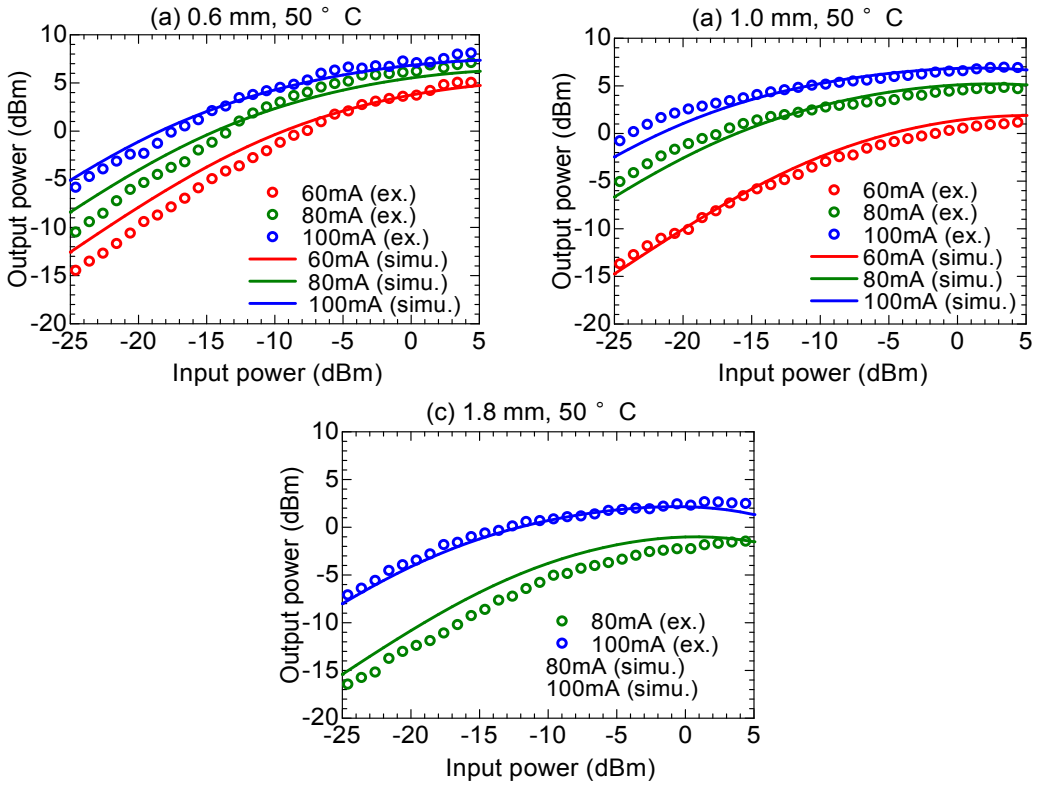

Fig. 3.10 Static input versus output characteristics of RSOA with length of 0.6 mm (a), 1.0 mm (b) and 1.8 mm (c) at the temperature of 50 °C. (ex.: experimental result, simu: simulation result)

Tab. 3.2 Parameters used at temperature of 25 °C and 50 °C.

Parameter	**Symbol**	**Value @ 25℃**	**Value @ 50℃**
Gain constant	a	3.2×10^{-16} cm^{-3}	2.7×10^{-16} cm^{-3}
Carrier density at transparency	n_0	6.0×10^{17} cm^{-3}	6.9×10^{17} cm^{-3}
Nonradiative recombination rate	A	5.25×10^{8} s^{-1}	5.25×10^{8} s^{-1}
Bimolecular recombination rate	B	2.0×10^{-10} cm^{3}s^{-1}	2.0×10^{-10} cm^{3}s^{-1}
Auger recombination rate	C	1.2×10^{-28} cm^{6}s^{-1}	2.0×10^{-28} cm^{6}s^{-1}
Self-saturation coefficient	ε_{11}	1.1×10^{-16} cm^{3}	0.9×10^{-16} cm^{3}
Cross-saturation coefficient	ε_{12}	2.2×10^{-16} cm^{3}	1.8×10^{-17} cm^{3}
Inversion factor	n_{sp}	1.6	1.4
Fiber coupling loss	L_c	5 dBm	2 dBm

3.5 Numerical prediction

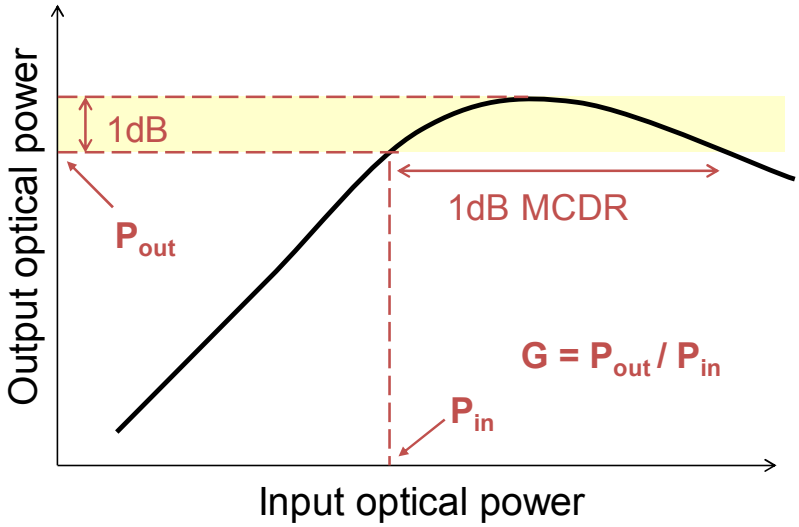

Fig. 3.11 Definition of evaluation parameters.

Using the numerical model and parameters derived in the previous section, we then carry out more comprehensive analysis to find the optimal RSOA design. For the quantitative and efficient evaluation of the modulation-canceling effect, we introduce three measures of performance as defined schematically in Fig. 3.11: 1-dB modulation cancellation dynamic range (MCDR), required input power Pin, and the corresponding optical gain G. 1 dB MCDR is defined to be the region of input power, within which the output power has less than 1-dB variation. This parameter evaluates how large and how flat the saturation region is. The optical input power and optical gain is defined at the starting point of MCDR. For WDM- PON application shown in Fig. 1, it is important to achieve large MCDR, low Pin, and large G for wide range of injected current, so that we can erase the modulated data of the incoming signal completely and reuse the light for upstream transmission.

Therefore, according to the objective, we need to know the MCDR, Pin and G of RSOA with different length and various level of injected current. We use our numerical model with the derived parameters to sweep different combinations of RSOA length and injected current, in each combination, we can obtain a curve as define in Fig, then we calculate respective MCDR, Pin and G, finally, we summarize the numerical results into 2D color maps as shown in Fig. 3.12.

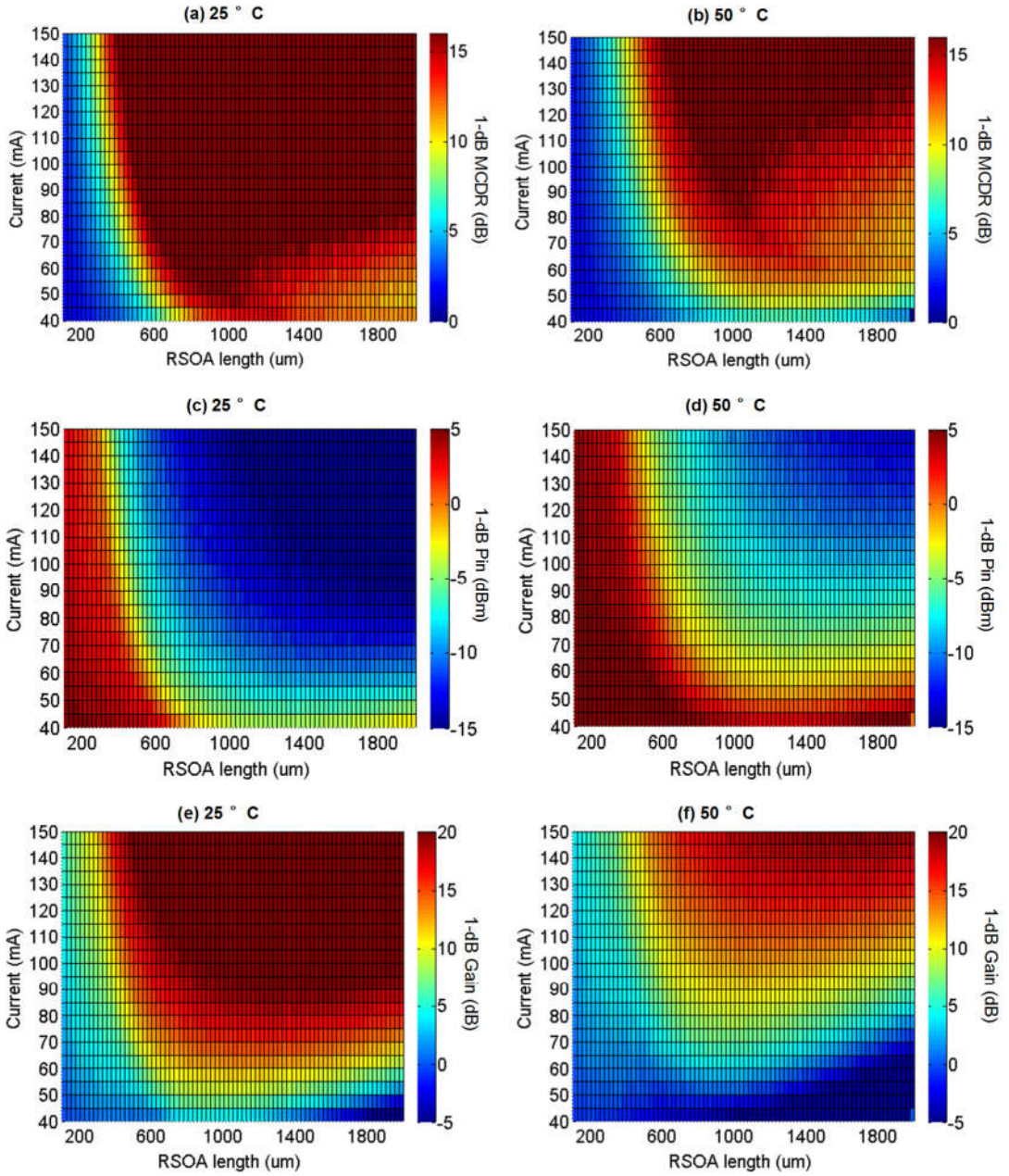

Fig. 3.12 Simulated results of MCDR (a,b), optical input power (c,d), optical gain (e,f) at temperature of 25 °C (a,c,e) and 50 °C (b,d,f).

The horizontal is the RSOA lengths swept from 100 to 2000 um, and longitudinal coordinate is injected current swept from 40 mA to 150mA. The color shows the value of derived parameters.

At each temperature, these figures indicate that: (i) the MCDR increases rapidly over 10 dB when the RSOA is longer than 0.6 mm, i.e. the RSOA length should at least

be longer than 0.6 mm for self-seeded operation, (ii) large MCDR is achieved for wide range of bias current, with the RSOA length around 1.0 mm. (iii) at longer length, both MCDR and G decrease gradually and Pin increases.

Comparing three parameters at two temperatures, there is a relatively large range of length and bias current at 25 °C to achieve the requirements. On the other hand, at 50 °C, the appropriate region of length shrinks but still centralized at the length of 1.0 mm.

In sum, the numerical analysis indicates that the RSOA length needs to be around 1.0 mm to achieve large MCDR, low Pin and large G in the wide range of bias current and temperature.

Chapter 4

System Experiments on RSOA

In order to verify our numerical prediction derived in last chapter, in this chapter, we experimentally compared the performance of RSOA with different length (0.6-mm, 1.0-mm, 1.6-mm) in a 2.5 Gb/s self-seeded subsystem at 25 °C and 50 °C. Then, we apply the confirmed optimal length to an amplified self-seeded system to achieve higher temperature (70 °C) and higher data rates (10 Gb/s).

4.1 Experiments of 2.5Gb/s Self-seeded system

4.1.1 Modulation characteristics of RSOA at 25 °C

We first try the data rate of 2.5Gb/s at 25 °C and compare the modulated output from RSOAs with different length.

Fig.4.1 shows the experimental setup. The RSOA was modulated at 2.5 Gb/s with a 2^{31}-1 pseudorandom bit sequence (PRBS) pattern. A 10 dB coupler is used to guide 90% of light goes into the reflective path comprised by circulator and polarization controller (PC), and the rest 10% of light goes to the measurement part. The PC was tuned to maximize the output power of the self-seeded cavity. The AWG exhibited Gaussian-profile with 100-GHz spacing. The round trip optical loss in the self-seeded cavity including AWG, coupler, circulator, and polarization controller was 12 dB. In the measurement part, we use two isolators before light goes into the switch to avoid light being reflected back into the main loop. One port of the switch is used for monitoring the optical spectrum and power of the output light, the other port is used for measuring the eye diagram and bit error rate.

With this system, we examine the influence of RSOA length (0.6 mm, 1.0 mm and 1.8 mm) on the modulation characteristics of self-seeded subsystem. For each sample, we carefully tune the bias current and peak-to-peak voltage of imposed data to achieve lowest BER.

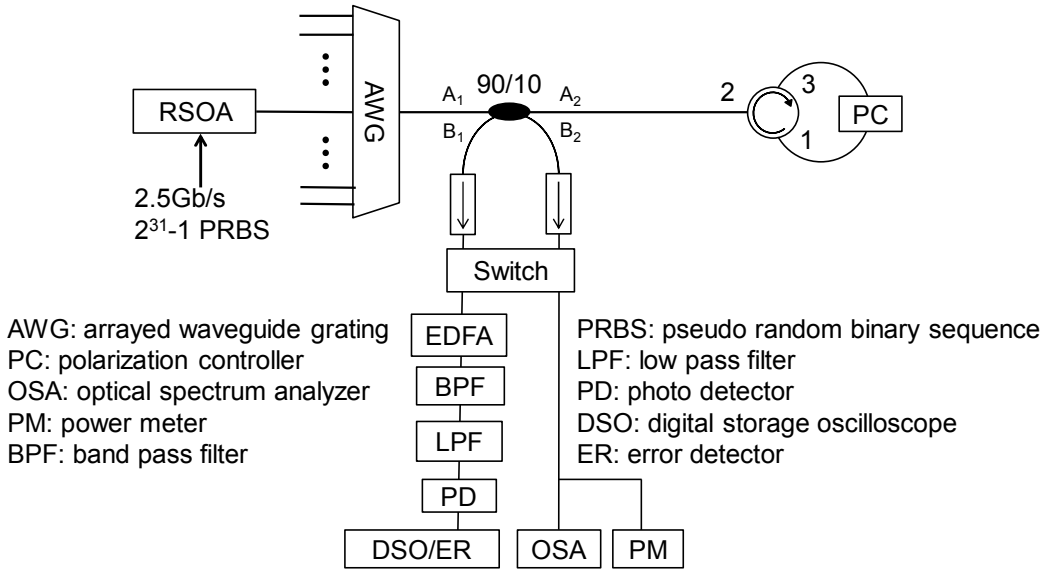

Fig. 4.1 Experimental setup

At first, we only add direct current to RSOA to investigate the output light of RSOA with different lengths. The results are shown in Fig. 4.2. In these figures, the loss of the measurement path has been calibrated, therefore the results show the optical spectra at B_2 port of the 10-dB coupler.

Different length shows different linewidth due to different longitudinal mode spacing. As show in fig.4.3, the free space range (FSR) is decreasing with the length increasing. For the length of 0.6 mm and 1.0 mm, there is only one mode can pass through the AWG, however, since the FSR of 1.8 mm is smaller than the passband of AWG, several modes can pass through, which results to the unstable mode hopping between several longitudinal modes, as a result, the full width at half maximum (FWHM) get broadened to 0.046 nm of 1.8-mm-long RSOA. For a system operation, obviously, one mode amplification and transmission is preferable for obtaining stable results.

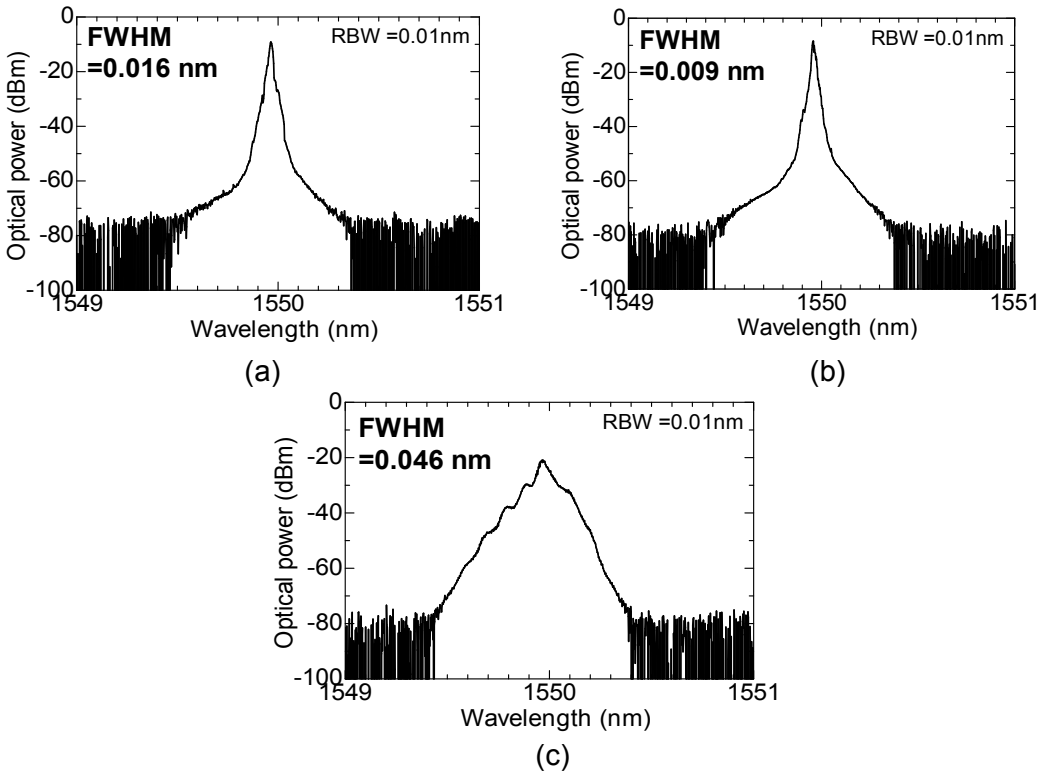

Fig. 4.2 Output light of RSOA without modulation of different length. (a) L = 0.6 mm, (b) L = 1.0 mm, (c) L = 1.8 mm.

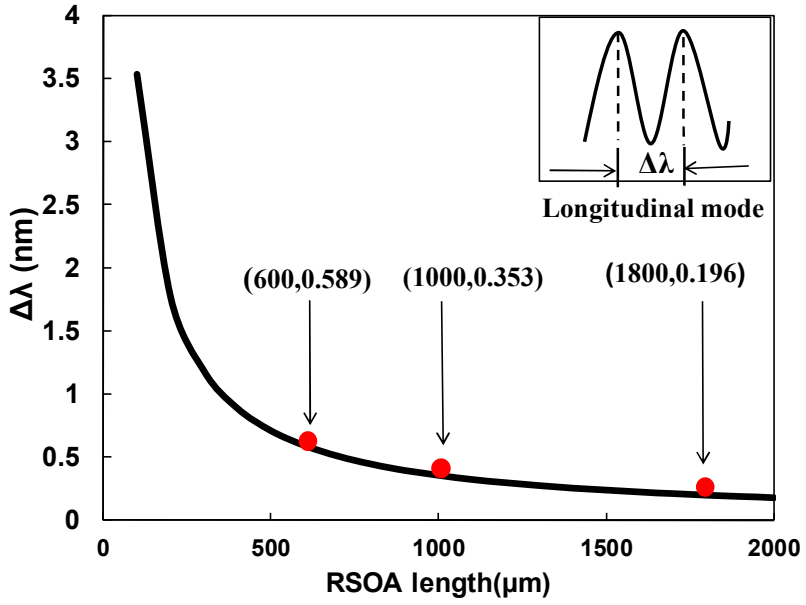

Fig. 4.3 Free space range in the function of RSOA length

Then we turn on the modulation. Fig. 4.4 shows the modulated optical spectra and the eye patterns as well as BER measured at output of RSOA (B_2 port in Fig.) at 25 °C for three RSOA samples with different length. The FWHM is minimized with the length of 1.0 mm due to the best suppression of relative intensity noise (RIN) which originates from the strong modulation canceling effect. The measured BER is the interactive results of modulation cancellation quality and remodulated extinction ratio (ER). In the eye diagrams in fig., in spite of the 1.8-mm-long RSOA has largest ER, 1.0-mm-long RSOA performs lowest BER. The BER characterization will be introduced in next section together with the results of after transmission.

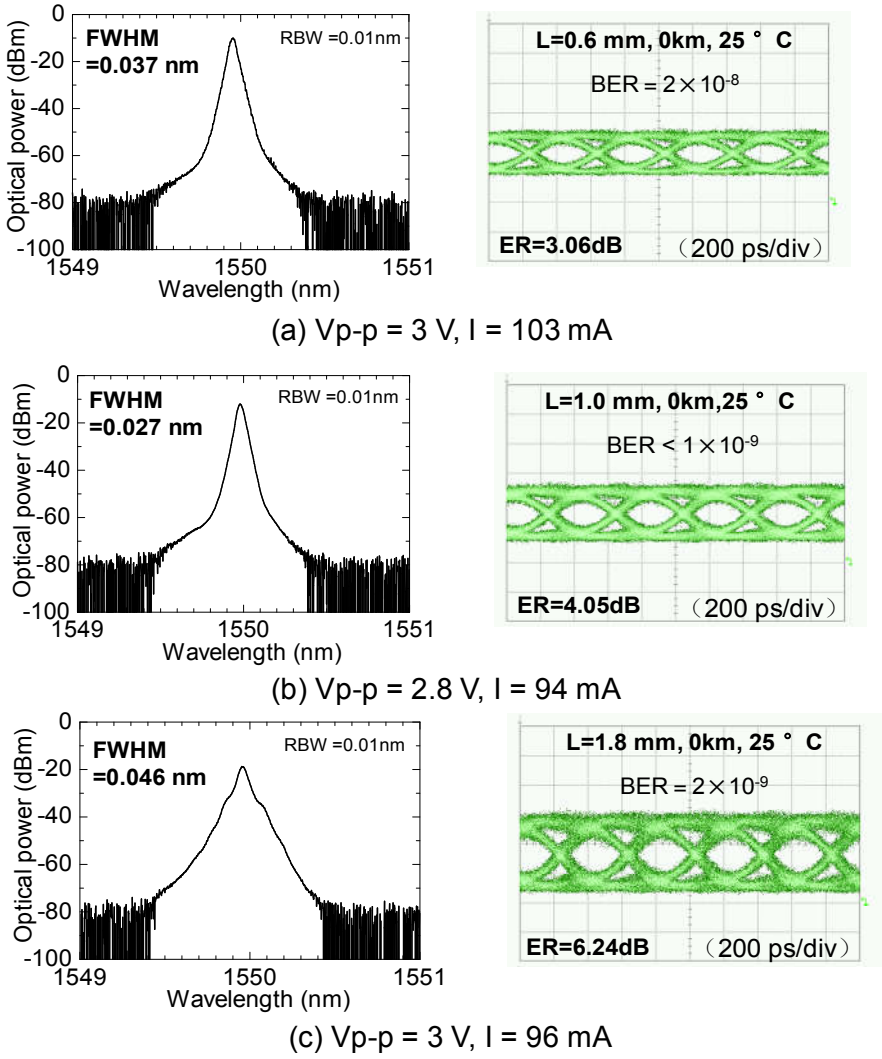

Fig. 4.4 Modulated spectra and eye diagrams of RSOA with length of (a) L = 0.6 mm, (b) L = 1.0 mm, and (c) L = 1.8 mm.

4.1.2 BER characterization of before and after 25-km SSMF Transmission

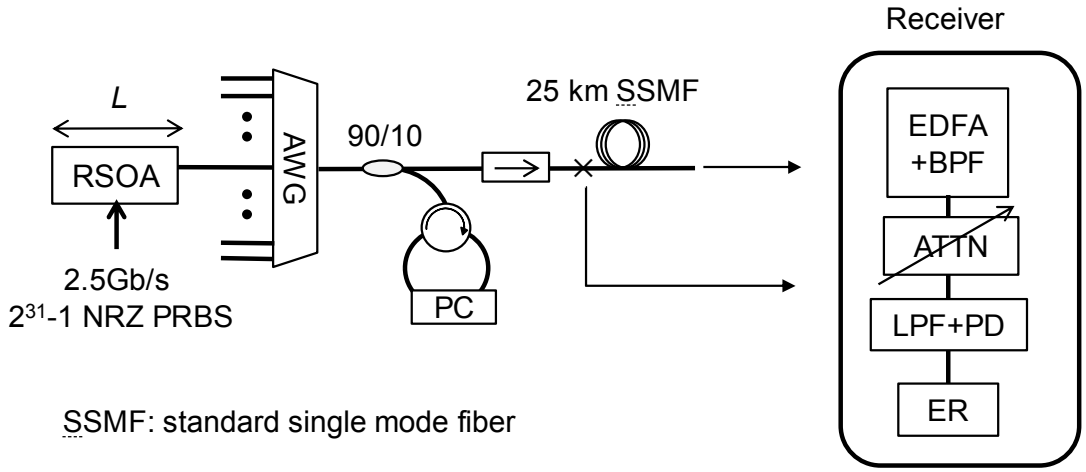

Fig. 4.5 Experimental setup of 25 km transmission

In the previous section, we have confirmed that 1.0-mm-long RSOA has best modulation characteristics. In this section, we compared the BER curve before and after 25-km standard single mode fiber transmission. Light from the self-seeded cavity is directed into an optical detector for characterization. The experimental setup is shown in Fig.4.5.

Fig.4.6 shows the measured the BER before and after transmission as a function of received power of the photon detector. At lower received power before transmission, the power penalty is minimized by using the 1.8-mm-long RSOA due to the fact that the ER is higher compared with that obtained by shorter RSOAs (refer to Fig. 4.4). However, at a higher receiver power, a noise floor emerges for the 1.8-mm-long RSOA, and the 1.0-mm-long RSOA exhibits the lowest BER. This is because the relative intensity noise (RIN) is smallest for the 1.0-mm-long RSOA due to the strongest modulation-cancellation effect, in agreement with the numerical results shown in Fig. 3.12. In the case of after transmission, the BER curves shown the same shape as that before transmission. In addition, 1.0-mm-long RSOA generally shows better stability than 1.8-mm-long RSOA, owing to the larger longitudinal mode spacing that avoids unstable mode-hopping.

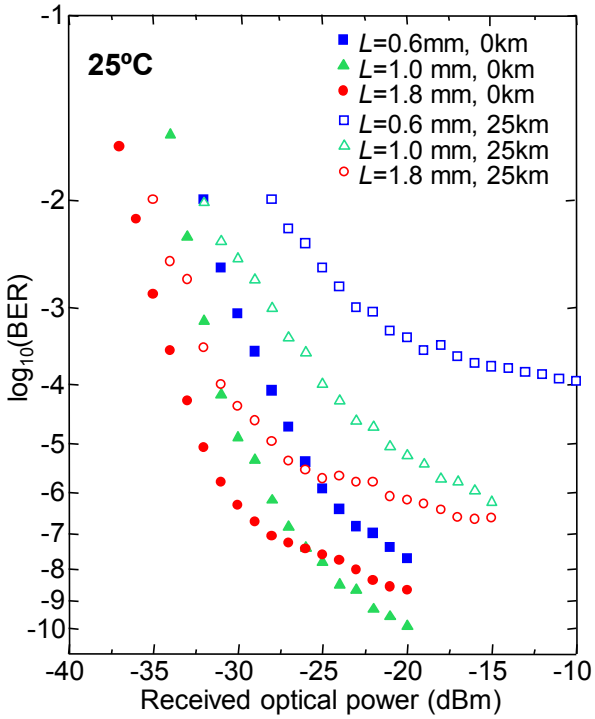

Fig. 4.6 Measured BER as a function of received power before and after transmission at 25 °C

4.1.3 Self-seeded system experiment at 50 °C

Then, we increase the temperature to 50 °C and repeat the previous measurements.

Fig.4.7 shows optical spectra and eye patterns of correspond RSOA length, 1.0-mm-long length still achieves the BER among them due to the best modulation cancellation at each level of modulated current. But in this case, in order to let 1.8-mm-long RSOA to achieve its best BER, we have to drastically decrease the $V_{p\text{-}p}$ to 1.3 V, which is the reason that 1.8-mm-long length has smaller FWHM than others. On the other hand, if we keep the $V_{p\text{-}p}$ of 1.8-mm-long RSOA as large as the other two lengths, then in eye pattern, we cannot observe any eye and cannot measure BER as shown in Fig. 4.7 (d). If we refer to the numerical results shown in Fig.3.12, at 50 °C, the MCDR of this length is large only at the very limited range of current, meaning we can only apply small $V_{p\text{-}p}$ to ensure modulation cancellation.

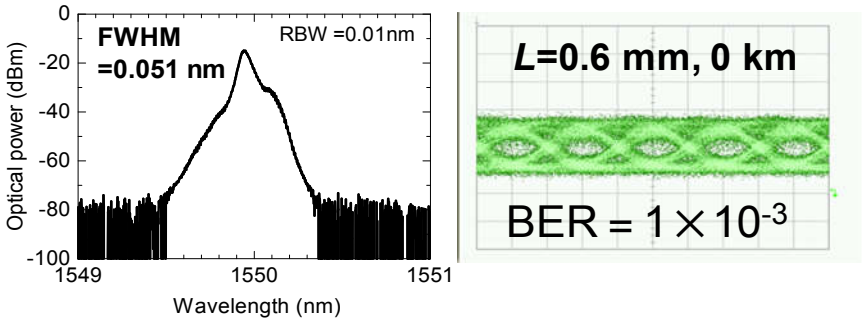

(a) Vpp = 2.9 V, I = 105 mA

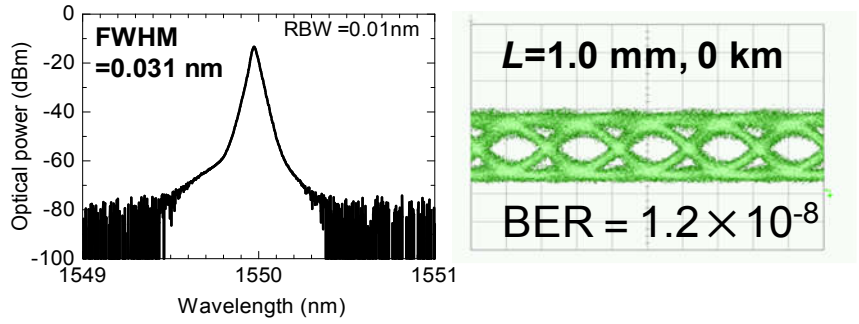

(b) Vpp = 2.6 V, I = 99 mA

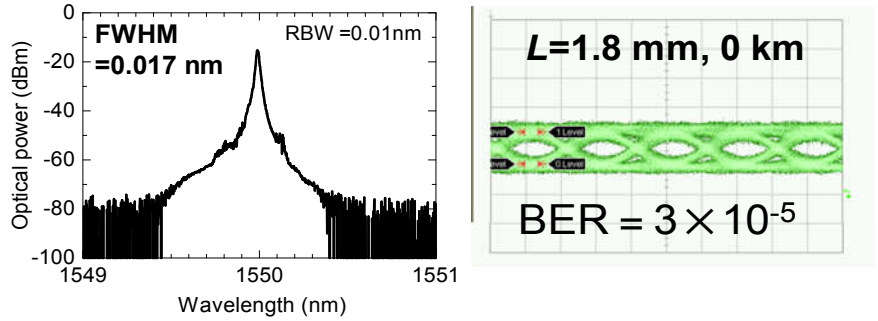

(c) Vpp = 1.3 V, I = 117 mA

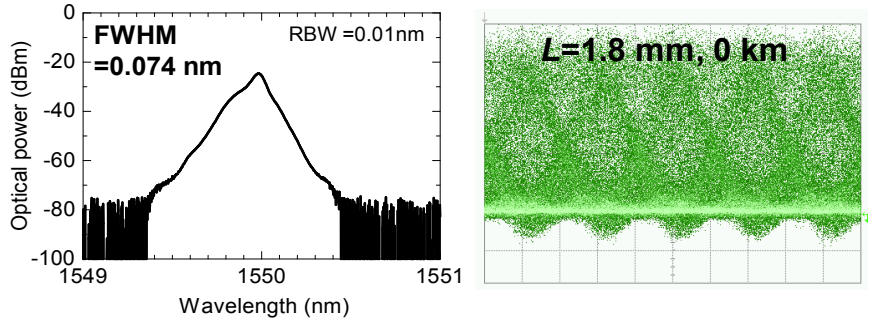

(d) Vpp = 2.6 V, I = 117 mA

Fig. 4.7 Modulated spectra and eye diagrams of RSOA with length of (a) L = 0.6 mm, (b) L = 1.0 mm, and (c,d) L = 1.8 mm at 50 °C

Finally, Fig. 4.8 show the measured BER curves at 50 °C. we didn't show the BER curve of 0.6 mm since even the best modulated output of this length can only achieve BER of 10^{-3} as shown in Fig.4.7 (a), decrease the received power or increase the transmission length will only worsen the BER. By using the 1.0-mm-long RSOA, we achieve transmission over 25-km SSMF with the BER below the forward-error-correction (FEC) limit of 10^{-4}. We only show the BER curve of 1.8-mm-long length before transmission since the BER before transmission is worse than that in 1.0-mm-long length after transmission.

As a result, the RSOA samples with L = 0.6 mm and 1.8 mm prohibit stable transmission due to small MCDR. These results are consistent with the numerical results in Fig. 3.12, which shows that a strong modulation cancellation effect is obtained at 50 °C only when the RSOA length is around 1.0 mm.

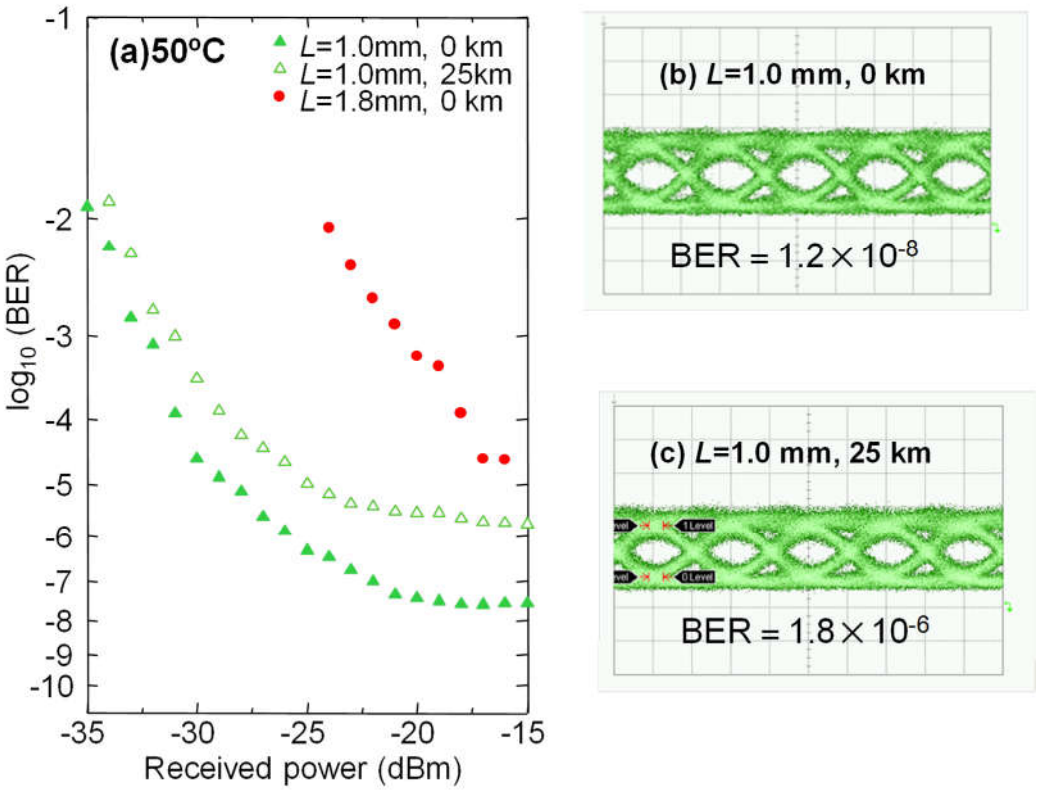

Fig. 4.8 Measured BER as a function of received power before and after transmission at 50 °C. (a) BER curves of three lengths, (b) Eye pattern of 1.0-mm-long length before and after transmission.

4.1.4. Summary of 2.5 Gb/s self-seeded system experiment at 25 °C and 50 °C

In previous sections, we have shown the detailed experimental results including optical spectra, eye diagrams and BER curves. To highlight our conclusions, we briefly summarize the results as following:

1. At 25 °C, both 1.0-mm-long and 1.8-mm-long shows good performance, our numerical results also show at room temperature, a relatively large range of length can have large MCDR.
2. At 50 °C, only 1.0-mm-long length has dominant advantages in achieving stable performance both before and after transmission.
3. Theoretically, 1.0-mm-long length should show better stability than longer length due to unstable mode hopping are easy to happen in longer length.
4. 1.0-mm-long length has larger gain than 1.8-mm-long length; therefore, 1.0-mm-long length should be better if we increase the length of distribution fiber. In practice, the distribution fiber should be longer than 1 km, in this situation, 1,8-mm-long length may not have enough gain to compensate the loss in the self-seeded cavity.

In all, both numerical and experimental results, and practical viewpoint indicate that 1.0-mm-long length is the optimal length for low-cost colorless self-seeded WDM-PON.

4.2 Limitations in the current self-seeded system.

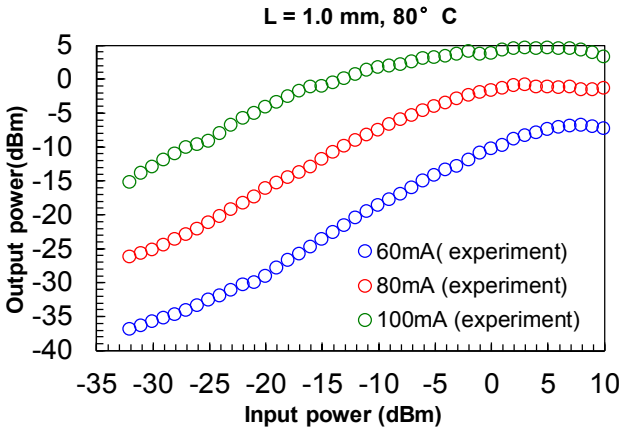

Fig. 4.9 Static input-output power curve for 1.0-mm-long RSOA at 80 °C

Tab. 4.1

Values of evaluation parameters for 1.0-mm-long RSOA at several levels of current.

Bias current	60mA	80mA	100mA
MCDR (dB)	5	11	13
Pin (dBm)	4.9	-0.1	-3.1
Gain (dB)	-13.31	-1.59	6.77

We also measure the characteristics of the optimal length at higher temperature, 80 °C. As shown in Fig.4.9 and Tab.4.1, at 80°C with bias current of 100mA, the MCDR is large enough but the optical gain at the starting point of MCDR is only around 7 dB. If we want to operate within the MCDR, the optical gain will be too low to compensate the round-trip loss (at least 12 dB). A method to overcome this is increasing to higher current to obtain higher gain. We believe at higher bias current, the optimal length in the self-seeded system is still hopeful to achieve uncooled operation. But the high frequency probe we used in the system prohibits higher current than ~110mA, therefore, we choose to improve the structure of self-seeded system.

4.3 Experiment of amplified self-seeded system

4.2.1 Amplified self-seeded system

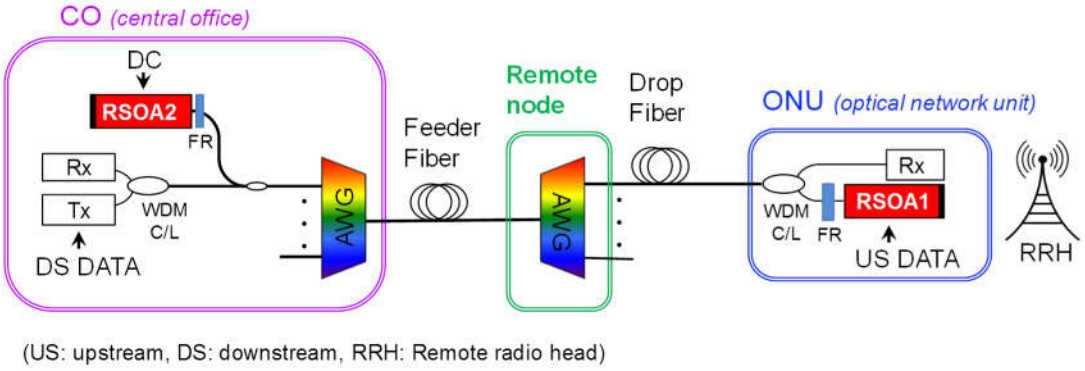

Fig. 4.10 Architecture of amplified self-seeded system [30].

The basic idea of amplified self-seeded system is that provide an amplification of the light in the cavity. Therefore, we use two RSOAs, but the function and position of each RSOA is different.

The first RSOA is located at ONU as a directly modulated transmitter and amplifier, in which, high modulation bandwidth and high gain over wide temperature range are needed. But for this RSOA, we don't care about its modulation canceling effect anymore. On the other hand, the modulation canceling function is realized by the second RSOA with the optimal length located at central office. With these two RSOAs, an amplified self-seeded cavity is formed. The modulated light from RSOA1 partly enters into the receiver and the rest optical power goes into the RSOA2 being bleached into CW light, then this CW light reflected back into ONU for modulation.

In this structure, we actually separate the modulator and modulation-canceling component. Since the temperature in the central office is stable than that in ONU, the modulation cancelling effect can always be ensured. Therefore, if the RSOA1 has high modulation bandwidth and good temperature characteristics, then uncooled and high data rate transmission can be expected. Further, the advantage of separating into two components is that we can optimize each for the best of its function.

In this proposed system [30], RSOA 1 has high polarization dependent gain (HPDG) and RSOA 2 has low polarization dependent gain (LPDG), two Faraday

rotators in the output port of RSOAs are used to keep the polarization state of incoming light and make sure the polarization is aligned to the high gain transverse mode of RSOA [31].

4.2.2 2.5 Gb/s modulation with amplified self-seeded subsystem at 70 °C

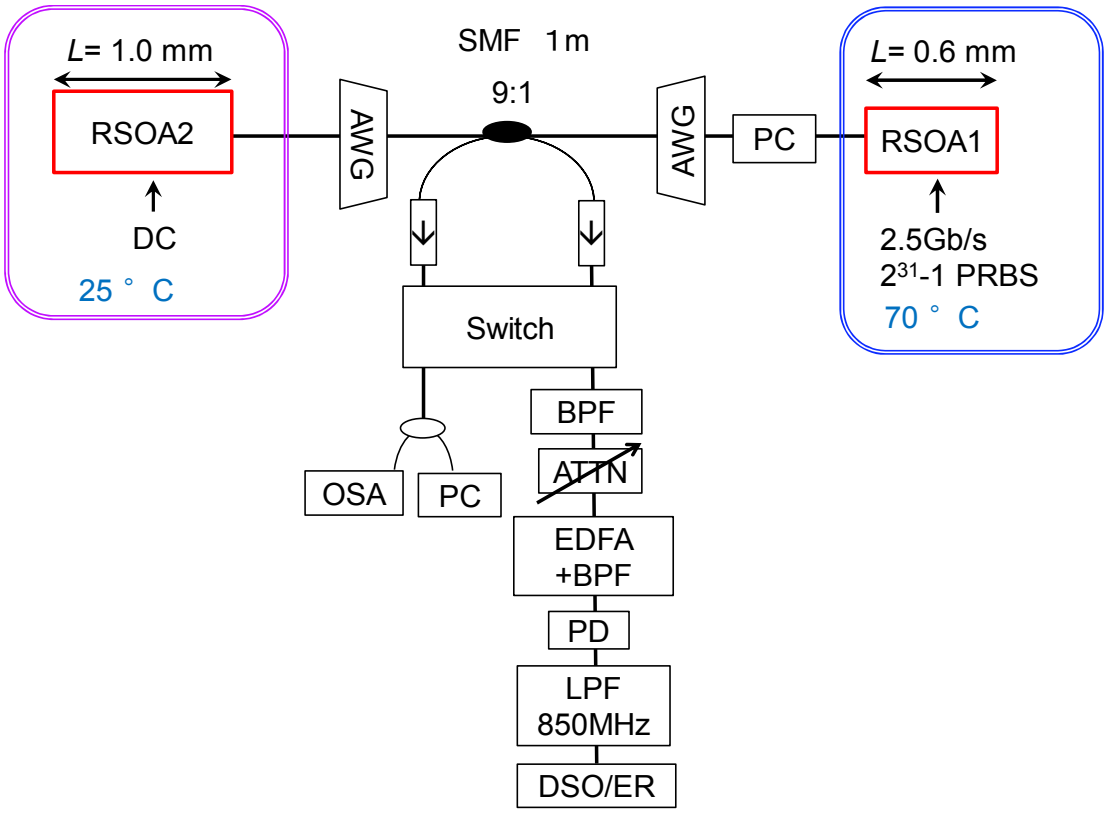

Fig. 4.11 Experimental setup for 2.5 Gb/s self-seeded system at 70 °C

We first carry out an experiment of 2.5 Gb/s at 70 °C with this amplified self-seeded system as shown in Fig.4.11. The RSOA 1 is operated at 70 °C, the length is 0.6-mm-long. This length has weak gain saturation therefore largest amplification of incoming light among three RSOA chips we have. The RSOA 2 is operated at room temperature, and the length is the derived optimal one, 1.0 mm. We inject data into

RSOA1 as it performs as the modulator, and we only inject DC bias to RSOA2 since it acts as a modulation canceling component.

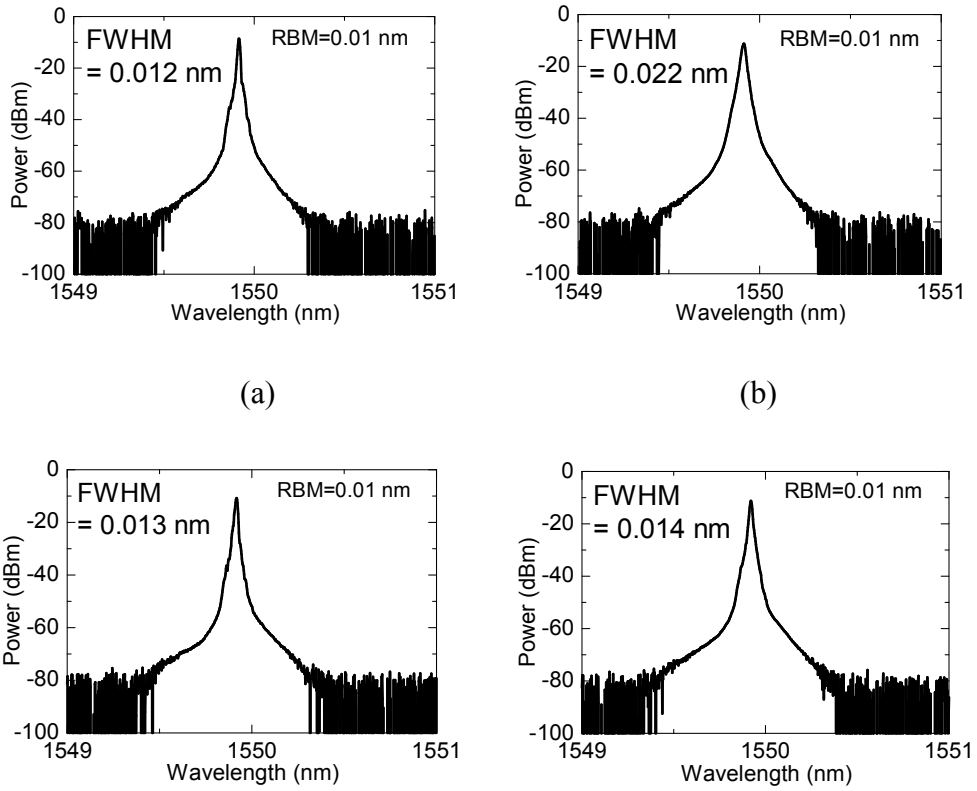

(a) (b)

(c) (d)

Fig. 4.12 Optical spectra from RSOA1 (transmitter) (a) without modulation, (b) with modulation. Optical spectra from RSOA2 (modulation canceling component) (c) without modulation, (d) with modulation.

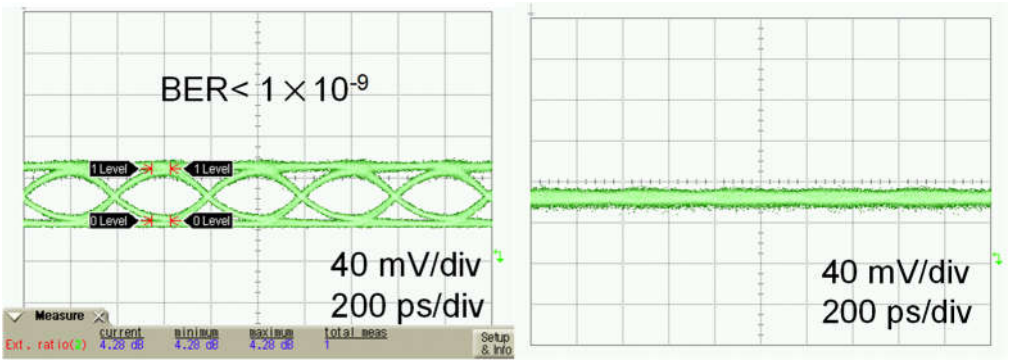

(a) (b)

Fig.4.13 Eye pattern from RSOA 1 (transmitter) (a) and from RSOA2 (modulation canceling component) (b) at 70 °C with data rate of 2.5 Gb/s.

Comparing the optical spectra from each RSOA with and without turning on the modulation in Fig. 4.12, we found that light from RSOA2 has small spectrum broaden because the modulation has been cancelled by the RSOA2.

Then we measure the eye pattern from each RSOA as shown in Fig.4.13. From RSOA1, the eye pattern from RSOA1 is very clear and achieves error free modulation. From RSOA2, the eye is completely closed due to good modulation canceling effect.

Therefore, this amplified system can easy to achieve uncooled operation at 2.5 Gb/s, but it is not so cost-efficient to only achieve this data rate by using two RSOAs. It can make more sense if this system can be modulated at 10 Gb/s.

4.2.3 10 Gb/s modulation with amplified self-seeded subsystem at 25 °C

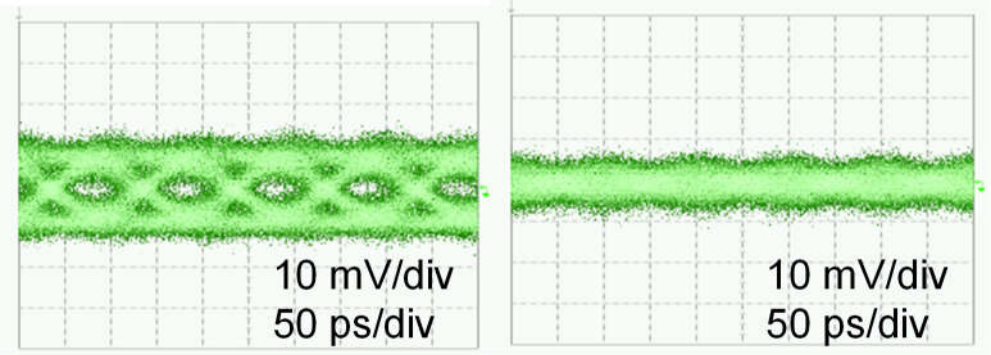

(a) (b)

Fig.4.14 Eye patterns from RSOA 1 (transmitter) (a) and from RSOA2 (modulation canceling component) (b) at 25 °C with data rate of 10 Gb/s.

With the same experimental setup, we increase the data rate to 10Gb/s. Both RSOAs are operated at room temperature. In Fig.4.14, we observe eye opening from RSOA1 and eye closure from RSOA2 but both of them look noisy, this is due to the limited modulation bandwidth of RSOAs we have. Usually, RSOAs chips have narrow bandwidth of ~2 GHz. It is enough for 2.5 Gb/s modulation but extremely limited for 10Gb/s data rate.

The reason of the limited bandwidth in RSOA compared to laser is that in a laser, only small part of light (1%) is emitted outside, the photon density inside cavity is always very high, therefore, the modulation bandwidth is mainly determined by the

electrical response, i.e. RLC response of laser. In addition, the frequency resonance appeared in laser response will increase the modulation bandwidth. However, in a RSOA, the photon density is not as high as that in a laser, the modulation bandwidth is mainly determined by the carrier lifetime in the cavity which can be estimated in the following equation [32]:

$$\frac{1}{\tau_{eff}} = A + BN + CN^2 + \Gamma a S v_g$$

Where the first term in the right hand side is carrier lifetime due to natural decay, and the second term is the carrier depletion due to stimulated emission. When the input power is large enough, we can ignore the first term, therefore, the carrier lifetime is mainly determined by the photon density in the cavity. RSOA does not have very high photon density since only a round-trip amplification and then most light are emitted out.

To overcome the limited bandwidth, design for large modulation bandwidth RSOA might be needed. Alternatively, we can employ some techniques to compensate for the limited bandwidth such as electronics equalizer, advanced modulation formats and so on [33,34].

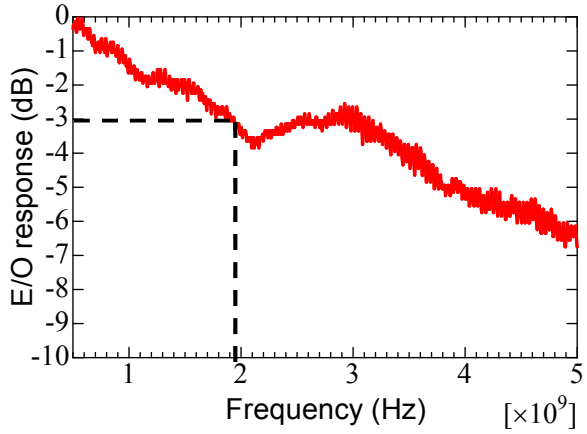

Fig.4.14 Measured 3-dB E/O response of RSOA chips with length of 0.6-mm-long

Chapter 5

Conclusions

In this study, we introduced self-seeded RSOA as a low-cost colorless transmitter at ONU, it has robust self-tunablity and has potential to achieve uncooled operation with optimized WDM-PON system.

We have introduced that the modulation canceling effect is the key for high speed modulation of self-seeded system. Also, the underlying physics behind modulation canceling effect has been clarified.

Our motivation is to explore the potential of RSOA for self-seeded applications as much as possible. Accurate and purposive design of RSOA can enhance the modulation canceling effect.

To achieve our objective, we built an accurate model to analyze the wave propagation process associated with carrier variation inside RSOA to reproduce the gain saturation effect. We numerically predicted that there exists an optimal RSOA length (1.0 mm) that can have large modulation canceling effect over wide current and temperature range (25 °C to 50 °C). Then we verified that this optimal length has best modulation canceling effect at self-seeded system at 25 °C and 50 °C.

For higher temperature and higher speed transmission, we introduced the amplified self-seeded system. With the derived optimal length, we easily achieved modulation at 70 °C. We observed eye opening at 10 Gb/s data rate. Better performances are expected by utilizing RSOA with higher modulation bandwidth or compensation techniques.

Bibliography

[1] Fukuchi, K., Kasamatsu, T., Morie, M., Ohhira, R., Ito, T., Sekiya, K., Ogasahara, D., Ono, T. "10.92-Tb/s (273 x 40-Gb/s) triple-band/ultra-dense WDM optical-repeatered transmission experiment." Optical Fiber Communication Conference. Optical Society of America, 2001.

[2] Oakley, K. A. "An economic way to see in the broadband dawn [passive optical network]." Global Telecommunications Conference, 1988, and Exhibition.'Communications for the Information Age.'Conference Record, GLOBECOM'88., IEEE. IEEE, 1988.

[3] Kazovsky, L. G., Shaw, W. T., Gutierrez, D., Cheng, N., & Wong, S. W. "Next-generation optical access networks." Lightwave Technology, Journal of 25.11 (2007): 3428-3442.

[4] Urata, R., Lam, C., Liu, H., & Johnson, C. "High performance, low cost, colorless ONU for WDM-PON." National Fiber Optic Engineers Conference. Optical Society of America, 2012.

[5] Wong, E. "Next-generation broadband access networks and technologies." Lightwave Technology, Journal of 30.4 (2012): 597-608.

[6] Kamei, S. "Recent progress on athermal AWG wavelength multiplexer." Optical Fiber Communication Conference. Optical Society of America, 2009.

[7] Banerjee, A., Park, Y., Clarke, F., Song, H., Yang, S., Kramer, G., Kim, K., & Mukherjee, B. "Wavelength-division-multiplexed passive optical network (WDM-PON) technologies for broadband access: a review [Invited]." Journal of optical networking 4.11 (2005): 737-758.

[8] Chang-Hasnain, Connie J. "Progress and prospects of long-wavelength VSELs." Communications Magazine, IEEE 41.2 (2003): S30-S34.

[9] Oh, S. H., Yoon, K. H., Kim, K. S., Kim, J., Kwon, O., Oh, D. K., Noh, Y.O., Seo, J.K., & Lee, H. J. "Tunable external cavity laser by hybrid integration of a

superluminescent diode and a polymer Bragg reflector." Selected Topics in Quantum Electronics, IEEE Journal of 17.6 (2011): 1534-1541.

[10] Tohmori, Y., Yoshikuni, Y., Ishii, H., Kano, F., Tamamura, T., Kondo, Y., & Yamamoto, M. "Broad-range wavelength-tunable superstructure grating (SSG) DBR lasers." Quantum Electronics, IEEE Journal of 29.6 (1993): 1817-1823.

[11] Ishii, H., Kano, F., Tohmori, Y., Kondo, Y., Tamamura, T., & Yoshikuni, Y. "Narrow spectral linewidth under wavelength tuning in thermally tunable super-structure-grating (SSG) DBR lasers." Selected Topics in Quantum Electronics, IEEE Journal of 1.2 (1995): 401-407.

[12] Kim H D, Kang S G, Le C H. A low-cost WDM source with an ASE injected Fabry-Perot semiconductor laser[J]. Photonics Technology Letters, IEEE, 2000, 12(8): 1067-1069.

[13] Healey, P., Townsend, P., Ford, C., Johnston, L., Townley, P., Lealman, I., Rivers, L., Perrin, S. & Moore. "Spectral slicing WDM-PON using wavelength-seeded reflective SOAs." Electronics Letters 37.19 (2001): 1.

[14] Nguyen, Truong An, Kim Lefebvre, and Leslie Rusch. "Multi-service OFDM Uplink Transmission in Full-Duplex FTTx Systems Using RSOA-based WDM-PON Architecture." Optical Fiber Communication Conference. Optical Society of America, 2014.

[15] Dúill, S. Ó., Marazzi, L., Parolari, P., Brenot, R., Koos, C., Freude, W., & Leuthold, J. "Efficient modulation cancellation using reflective SOAs." Optics express 20.26 (2012): B587-B594.

[16] Garces, I., Aguado, J. C., Martinez, J. J., Lopez, A., Villafranca, A., & Losada, M. A. "Analysis of narrow-FSK downstream modulation in colourless WDM PONs." Electronics Letters 43.8 (2007): 1.

[17] Wong, E., Lee, K. L., & Anderson, T. B. "Directly modulated self-seeding reflective semiconductor optical amplifiers as colorless transmitters in wavelength division multiplexed passive optical networks." Journal of Lightwave Technology 25.1 (2007): 67-74.

[18] Kang, J. M., Kim, T. Y., Choi, I. H., Lee, S. H., & Han, S. K. "Self-seeded reflective semiconductor optical amplifier based optical transmitter for up-stream WDM-PON link." Optoelectronics, IET 1.2 (2007): 77-81.

[19] Brenot, R. "Demystification of Self-Seeded WDM Access." Optical Fiber Communication Conference. Optical Society of America, 2015.

[20] Parolari, P., Marazzi, L., Brunero, M., Martinelli, M., Brenot, R., Maho, A., ... & Chanclou, P. "10-Gb/s operation of a colorless self-seeded transmitter over more than 70 km of SSMF." Photonics Technology Letters, IEEE 26.6 (2014): 599-602.

[21] Sato, K., & Toba, H. "Reduction of mode partition noise by using semiconductor optical amplifiers." Semiconductor Laser Conference, 2000. Conference Digest. 2000 IEEE 17th International. IEEE, 2000.

[22] Connelly, Michael J. "Wideband semiconductor optical amplifier steady-state numerical model." (2001).

[23] Coldren, L. A., Corzine, S. W., & Mashanovitch, M. L. Mashanovitch. “Diode lasers and photonic integrated circuits”. Second Edition. John Wiley & Sons, 2012.

[24] Cheng, N., & Kazovsky, L. G. "Implications of injection current and optical input power on the performance of reflective semiconductor optical amplifiers." Integrated Optoelectronic Devices 2007. International Society for Optics and Photonics, 2007.

[25] de Melo, A. M., & Petermann, K. "On the amplified spontaneous emission noise modeling of semiconductor optical amplifiers." Optics Communications 281.18 (2008): 4598-4605.

[26] Y. Zeng, “Research on Reflective Semiconductor Optical Amplifier and Its Application in Wavelength Division Multiplexed Passive Optical Network” Master thesis, Department of Electrical Engineering and Information Systems, the University of Tokyo, 2013.

[27] Agrawal, G. P., & Olsson, N. A. "Self-phase modulation and spectral broadening of optical pulses in semiconductor laser amplifiers." Quantum Electronics, IEEE Journal of 25.11 (1989): 2297-2306.

[28] Agrawal, G. P. "Fiber-optic communication systems." Third Edition, John Wiley & Sons, Inc. (2002).

[29] Zah, C. E., Bhat, R., Pathak, B., Favire, F., Wang, M. C., Lin, W., ... & Wang, Z. "High-performance uncooled 1.3-μm AlGaInAs/InP strained-layer quantum-welllasers forfiber-in-the-loop applications', ThG1." Tech. Dig. OFC 94 (1994): 204-205.

[30] Parolari, P., Marazzi, L., Brunero, M., Gatto, A., Martinelli, M., Brenot, R., ... & Barbet, S. "10-Gb/s amplified self-seeding WDM PON transmission exploiting RSOAs." Networks and Optical Communications-(NOC), 2014 19th European Conference on. IEEE, 2014.

[31] Martinelli, M., Marazzi, L., Parolari, P., Brunero, M., & Gavioli, G. "Polarization in retracing circuits for WDM-PON." Photonics Technology Letters, IEEE 24.14 (2012): 1191-1193.

[32] de Valicourt, G. Next Generation of Optical Access Network Based on Reflective-SOA. INTECH Open Access Publisher, 2012.

[33] Papagiannakis, I., Omella, M., Klonidis, D., Birbas, A. N., Kikidis, J., Tomkos, I., & Prat, J. "Investigation of 10-Gb/s RSOA-based upstream transmission in WDM-PONs utilizing optical filtering and electronic equalization." Photonics Technology Letters, IEEE 20.24 (2008): 2168-2170.

[34] Omella, M., Polo, V., Lazaro, J., Schrenk, B., & Prat, J.. "10 Gb/s RSOA transmission by direct duobinary modulation." 2008 34th European Conference on Optical Communication. 2008.

List of Publications

Journal Paper

[1] Zhan W., Tanemura T., Yamauchi S., Mukaikubo M. & Nakano Y. “Optimal design of Self-seeded Reflective Semiconductor Optical Amplifier for Low-cost WDM-PON”, Journal of Lightwave Technology. In preparation.

Conference papers

[1] Zhan W., Tanemura T., Zeng Y., Yamauchi S., Mukaikubo M. & Nakano Y. “Optimization of RSOA for Self-Seeded Colorless WDM-PON Transmitters”, The Institute of Electronics, Information and Communication engineers, C-4-15,立命馆大学,日本（2015.2).

[2] Zhan W., Tanemura T., Zeng Y., Yamauchi S., Mukaikubo M. & Nakano Y. “Optimization of 1.55um InGaAlAs/InP MQW-RSOA for Self-Seeded Colorless WDM Transmitter”. Compound Semiconductor Week 2015, Santa Barbara, CA. O7.4 (2015.7).

[3] Zhan W., Tanemura T., Yamauchi S., Mukaikubo M. & Nakano Y. “High-Temperature Operation of Self-seeded RSOA for Low-Cost WDM-PON Transmitters”, The Institute of Electronics, Information and Communication engineers, B-10-70, 东北大学,日本（2015.9）.

[4] Zhan W., Tanemura T., Yamauchi S., Mukaikubo M. & Nakano Y. “Uncooled (25 - 50 deg C) Operation of Self-Seeded RSOA for Low-Cost Colorless WDM-PON Transmitter”. European Conference on Optical Communication, Valencia, Spain, We.1.5.5 (2015.9).

[5] Zhan W., Tanemura T., Yamauchi S., Mukaikubo M. & Nakano Y. “Optimization of Self-seeded Reflective-SOA for Low-cost Colorless WDM-PON Transmitters”, 通信方式/光通信システム研究会, 鹿児島大学　日本 (2016.1)

Acknowledgement

This thesis would not have been possible without the help of so many people.

I would like to express my deepest appreciation to my supervisor, Professor Yoshiaki Nakano, who accepted me as a member in his group and provide such a great circumstance to do research. Thank him for giving me precious guidance and advice at each stage of my research.

I would like to thank Associate Professor Takuo Tanemura, who introduced this interesting topic to me and gave me kind guidance and persistent help as well as providing precious information regarding this research. Without his guidance in experiment, simulation and paper writing, I could not have the chance to attend international conference during the master's course.

I want to express my thanks to Kazuhisa Uomi, Hiroaki Inoue, Takayoshi Fukui, Kenji Uchida, Masaru Mukaikubo from Oclaro Japan, Inc. for providing the RSOA samples and giving me helpful advice in the meeting.

I also would like to take this opportunity to record my sincere thanks to Associate Professor Masakazu Sugiyama and all the members in Nakano& Sugiyama &Tanemura lab for their kind help and encouragement.

Finally, thanks to my parents, who support my life in Japan and comfort me every time when I feel difficult. Thanks to my husband, who go through all the happiness and sadness with me.

Zhan Wenhui
January 2016